Comparison of Transmission Characteristics of Add-drop Ring Resonators with Different Geometric Shapes

SUBMITTED BY

Rashadul Hasan Badhon (Student ID-132413)

Md. Faiyaz Kabir (Student ID-132417)

Ann-noor Bhuiyan Rijhum (Student ID-132419)

MD.Zahirul Islam Khan (Student ID-132485

A Thesis Submitted to the Academic Faculty in Partial Fulfillment of the Requirements for the Degree of

BACHELOR OF SCIENCE IN ELECTRICAL AND ELECTRONIC ENGINEERING

Department of Electrical and Electronic Engineering

Islamic University of Technology (IUT)

Gazipur,Dhaka

Comparison of Transmission Characteristics of Add-drop Ring Resonators with Different Geometric Shapes

Approved By:

Rakibul Hasan Sagor
Thesis Supervisor,
Assistant Professor,
Department of Electrical and Electronic Engineering,
Islamic University of Technology.

Prof. Dr. Md. Ashraful Hoque
Head of the Department,
Department of Electrical and Electronic Engineering,
Islamic University of Technology.

Declaration of Authorship

We, Rashadul Hasan Badhon (132413), Md. Faiyaz Kabir (132417), Ann-noor Bhuiyan Rijhum (132419) and Md. Zahirul Islam Khan (132485) declare that this thesis titled, 'Comparison of Transmission Characteristics of Ring Resonators with Different Geometric Shapes' and the works presented in it are our own. We confirm that:

- This work has been done for the partial fulfillment of the Bachelor of Science in Electrical and Electronic Engineering degree at this university.
- Any part of this thesis has not been submitted anywhere else for obtaining any degree.
- Where we have consulted the published work of others, we have always clearly attributed the sources.

Submitted By:

_____

Rashadul Hasan Badhon (132413)

_____

Md. Faiyaz Kabir (132417)

_____

Ann-noor Bhuiyan Rijhum (132419)

_____

Md. Zahirul Islam Khan (132485)

Contents

List of figures

Abstract

Plasmonic devices have become a very popular topic of research in recent years due to their properties which allow them to outperform conventional electronic devices in many aspects, the most of important of which is their ability to overcome the diffraction limit. This allows Plasmonic devices to be miniaturized to the nanometer scale, which makes them extremely useful for various optical applications. Here, a special class of Plasmonic devices called add-drop ring resonators were investigated. Various configurations of these resonators with different geometric shapes for the ring were proposed. The transmission characteristics of these structures were analyzed and compared by carrying out simulations to calculate the transmission efficiency at the drop and through ports for different wavelengths of light. The effect on the transmission characteristics due to modifications in the structures were also observed. The add-drop ring resonator configurations with elliptical shaped ring and round-edge square shaped ring both performed better than the conventional circular ring design, exhibiting higher transmission efficiencies at the drop port.

Acknowledgements

We would like to offer our gratitude to the Almighty Allah (SWT) for giving us the good health and fortune needed to carry out this work.

We would like to thank our research supervisor, Rakibul Hasan Sagor sir, for the support and guidance he gave us throughout our research at Islamic University of Technology (IUT). He created a nice environment where we were able to explore many ideas without constraint. We have gained a wealth of knowledge and experience in science and engineering through his direction that is beyond value to our future endeavor. For all of his efforts as true mentor, we express our heartfelt gratitude to him.

We would like to thank all the faculty member of the Department of Electrical & Electronic Engineering (EEE) at Islamic University of Technology (IUT) for helping and inspiring us.

And finally, we would like thank our parents, our families, our relatives and our friends. Without them being in our lives, it would have been impossible for us to come this far.

Abbreviations

ABC	Absorbing Boundary Condition
ADE	Auxiliary Differential Equation
AlAs	Aluminum Arsenide
DMD	Dielectric-Metal-Dielectric
EM	Electromagnetic
FDTD	Finite Difference Time Domain
GLS	Gallium Lanthanum Sulfide
IR	Infra-Red
LD	Lorentz-Drude
MDM	Metal-Dielectric-Metal
PLRC	Piecewise Linear Recursive Convolution
PML	Perfectly Matched Layer
SPP	Surface Plasmon Polariton
TE	Transverse Electric
TM	Transverse Magnet

Chapter 1

Introduction and Background

In recent years, researches in optical devices have progressed rapidly due to the advantages they provide over electronic devices, which have been the most commonly used components for the construction and integration of miniaturized circuits [1]. Modern electronic devices are limited by the lack of speed and lower bandwidth. These problems can be overcome by using a class of optical devices called Plasmonic devices, which work on the principle of the propagation of Surface Plasmon Polariton (SPP) [2] waves. These devices not only provide faster speeds of operation and higher bandwidth [3], but also allow the miniaturization of devices to the nanometer scale [4] by allowing the confinement of electromagnetic waves over dimensions in the nanometer range [5, 6]. These devices are very versatile and they can be used in many useful applications such as filters [7-9], biosensors [10] and optical communication systems [11].

The performance, speed and ease-of-use of semiconductor devices, circuits and components is dependent on their miniaturization and integration into external devices. However, the integration of modern electronic devices for information processing and sensing is rapidly approaching its fundamental speed and bandwidth limitations, which is an increasingly serious problem that impedes further advances in many areas of modern science and technology. One of the most promising solutions is believed to be in replacing electronic signals (as information carriers) by light. However, a major problem with using electromagnetic waves as information carriers in optical signal-processing devices and integrated circuits is the low levels of integration and miniaturization available, which are far poorer than those achievable in modern electronics. This problem is a consequence of

the diffraction limit of light in dielectric media, which does not allow the localization of electromagnetic waves into nanoscale regions much smaller than the wavelength of light in the material.

The use of materials with negative dielectric permittivity is one of the most feasible ways of circumventing the diffraction limit and achieving localization of electromagnetic energy (at optical frequencies) into nanoscale regions as small as a few nanometers. The most readily available materials for this purpose are metals below the plasma frequency. Metal structures and interfaces are known to guide surface plasmon–polariton (SPP) modes, electromagnetic waves coupled to collective oscillations of electron plasma in the metal. As a result, plasmonics is an area of nanophotonics beyond the diffraction limit that studies the propagation, localization and guidance of strongly localized SPP modes using metallic nanostructures. The recent rapid development of plasmonic waveguides whose mode confinement is not limited by the material parameters of the guiding structure has been primarily driven by the tantalizing prospect of combining the compactness of an electronic circuit with the bandwidth of a photonic network.

Utilizing the beneficial property of plasmonic devices to overcome the diffraction limit, a lot of recent research has been carried out on a type of plasmonic nanostructure called a ring resonator [12]. Ring resonators have properties which causes the resonance of the light within the ring at different frequencies, depending on the structure of the resonator. One of the most important advantages provided by ring resonators is that they can be tuned easily [13], i.e. the resonant frequencies can be varied by changing the dimensions of the resonator. Ring resonators have numerous proposed and demonstrated applications in sensors [14], modulators [15], filters [16], laser systems [17], optical buffers [18], and interferometry, etc.

An add-drop ring resonator [19, 20] is a special type of ring resonator consisting of a looped dielectric waveguide coupled to two dielectric straight waveguides and surrounded by a

metal. The most commonly used ring resonator configuration has a circular ring coupled with waveguides. However, other configurations with various geometric variations of the structure have been researched to achieve better transmission characteristics and desired resonant properties, such as a hexagonal split ring resonator [21] and a UWB BPF using square ring resonator [22] etc. Modifications to ring resonator geometry and waveguide parameters can be analyzed to give the desired transmission characteristics for a particular optical application. The comparison between the transmission efficiencies and the resonant frequencies of these ring resonator structures can help determine which ones can be best used as filters and other plasmonic devices requiring a specific transmission characteristic.

1.1 Overview of Surface-Plasmon-Polariton

Surface plasmon polaritons are electromagnetic excitations propagating at the interface between a dielectric and a conductor, evanescently confined in the perpendicular direction. These electromagnetic surface waves arise via the coupling of the electromagnetic fields to oscillations of the conductor's electron plasma.

The eigenmodes of an interface between a dielectric and a metal are surface plasmon polaritons (SPPs) [23]. We refer to them as eigenmodes in the sense that they are solutions of Maxwell's equations that can be formulated in the absence of an incident field. On a flat interface between dielectric and metal half-spaces with dielectric constants ε_d and ε_m, respectively, SPPs are transverse magnetic (TM) plane waves propagating along the interface. Assuming the interface is normal to z and the SPPs propagate along the x direction, the SPP wave vector k_x is related to the optical frequency through the dispersion relation [24].

$$k_x = k_o\sqrt{\epsilon_d\epsilon_m/(\epsilon_d + \epsilon_m)} \tag{1.1}$$

where, $k_0 = \frac{\omega}{c}$ is the free-space wave vector. We take ω to be real and allow k_x to be complex, since our main interest is in stationary monochromatic SPP fields in a finite area [25]. The details of SPP has been discussed in Chapter 2.

1.2 Literature Review

Plasmonic ring resonators based on SPP wave propagation have been a great field of interest over the recent years. A number of researches have been carried out throughout recent years on the same topic. However, there's still huge scope for the researches in this field. Here in this section of literature review, focus have been made on the literature review of the published works on SPP propagation analysis through different structures with different geometries and most importantly, on ring resonators.

The parameters of several metals have been reported to our knowledge. Jin et al. [26] determined the modified Debye model parameters for gold which are applicable in the wavelength range of 550-950 nm. Krug et al. [27] reported the gold parameters that are applicable in the wavelength range of 700-1000 nm. W.H.P. Pernice et al. [28] extracted the parameters for Nickel using Lorentz-Drude model. A.D. Rakic et al. [29] reported the parameters for Nickel, Palladium, Titanium and 8 other metals using Lorentz-Drude and Brendel-Bormann Model. M.A. Ordal et al.[30] extracted the parameters for fourteen metals in the infrared and far-infrared range.

Bends, splitters and recombinations are inevitable parts of optoelectronic devices. Several works on the analysis of SPP propagation in these shapes have been reported to our knowledge. G. Veronis et al. [31] showed that bends and splitters can be designed over a wide frequency range without much loss by keeping centre layer thickness small compared to wavelength. H. Gao et al. [32] investigated the propagation and combination of SPP in Y-shaped channels. B. Wang et al. [33] analyzed two structures which consist of splitting and recombination.

The propagation loss of SPP is very high in metal-dielectric-metal configuration of plasmonic waveguide which limits the length of propagation. Even the fabrication related disorders have far less impact on the propagation loss than the losses that occur in metallic

layers of the MDM waveguide. This problem can be addressed by using both dielectric and plasmonic waveguide on the same chip. The dielectric waveguide will carry the fundamental optical mode while the plasmonic waveguide will address the sub-wavelength scale issue. This calls for the need of efficient coupling of optical modes from the dielectric waveguide to the plasmonic waveguide. Therefore, designing efficient nanoplasmonic couplers with different materials and structures can be a pioneering step in miniaturization of the integrated photonic devices. In the past years, several plasmonic couplers have been proposed by different researchers. G. Veronis et. Al. [34] proposed a coupler with multi-section tapers. P. Ginzburg et al. [35] reported a λ/4 coupler to couple optical modes from a 0.5m to 50nm wide plasmonic waveguide. D. Pile et al. [36] presented an adiabatic and a non-adiabatic tapered plasmonic coupler. R. Washleh et al. [37] reported an analysis on nanoplasmonic air-slot coupler and its fabrication steps.

For the design of plasmonic devices, metal-dielectric-metal (MDM) interfaces are very popular. Different types of structures have been proposed till now based on this MDM interface. Jacob Scheuer, Yoav Yadin and Moti Margalit proposed micro ring resonator structures which relates to optical cavity and more particularly to ring like cavities used in integrated optical devices. Add-drop multiplexer was introduced by Jun Su and Yi Ding which was later used in wavelength division multiplexed networks. Su and Ding proposed that in some embodiments, ring resonator may be used instead of Bragg gratings in a Mach-Zehnder interferometer configuration.

1.3 Thesis objective:

The main objective of this thesis is to design and compare plasmonic add-drop ring resonator structures of various geometric shapes. More specifically, the objectives are: -

- To develop a simulation model based on the FDTD method that is capable of simulating the devices.

- To analyze and compare the transmission characteristics of the designed Nano-

structures by measuring the power through different ports.

- To analyze important conclusions from the obtained results and discuss the potential applications.

1.4 Thesis organisation

The thesis has been arranged in the following way-

- In Chapter 2, the basic theory of SPP propagation has been described. This chapter introduces the fundamental knowledge and necessary mathematical formulations of SPP propagation at the single and double interface.
- In Chapter 3, the widely used models for modeling metals have been described in detail with necessary derivations. Since SPPs are created due to the coupling of photon energy to the free electrons of metal, modeling metals is one of the key steps for the simulation of SPP propagation.
- Since we have developed our simulation model based on FDTD method, Chapter 4 introduces the fundamentals of the FDTD algorithm for 1D and 2D simulations. The original formulations of Yee do not include the frequency dependent dispersion properties of materials. We have used the ADE based general algorithm for our simulation model which is discussed in Chapter 4. This chapter also discusses about the absorbing boundary condition.
- In chapter 5, the Lorentz model and the six-pole Lorentz model are discussed and also a developed simulation model is established
- In chapter 6 the design of add-drop ring resonators of various geometric shapes along with the Ex, Ey, Hz profiles on the Metal-Dielectric-Metal interfaces and the snapshots of Hz field is provided.
- In chapter 7 the transmission characteristics are analyzed and compared and the effect of increased coupling distance is also analyzed.
- In chapter 8, the results are summarized and a brief idea of our future work is given.

Chapter 2

SPP Propagation Theory

2.1 Introduction

Surface plasmon polariton (SPP) is an electromagnetic excitation that propagates in a wave like fashion along the planar interface between a metal and a dielectric medium, often vacuum, and whose amplitude decays exponentially with increasing distance into each medium from the interface. Electromagnetic wave propagation is obtained from the solution of Maxwell's equations in each medium, and the associated boundary conditions. Maxwell's equations of macroscopic electromagnetism can be written as follows:

From Gauss's Law for the electric field

$$\nabla . D = \rho_{ext} \tag{2.1}$$

From Gauss's Law for the magnetic field

$$\nabla . B = 0 \tag{2.2}$$

From Faraday's Law

$$\nabla \times E = -\frac{\partial B}{\partial t} \tag{2.3}$$

From Ampere's Law

$$\nabla \times H = J_{ext} + \frac{\partial D}{\partial t} \tag{2.4}$$

Here,

E is the electric field vector in Volt per meter

D is the electric flux density vector in Coulombs per square meter

H is the magnetic field vector in Amperes per meter

B is the magnetic flux density vector in Webers per square meter

J_{ext} is the current density

The four macroscopic fields can be also linked further via the polarization P and magnetization M by

$$D = \varepsilon_0 E + P \tag{2.5}$$

$$H = \frac{1}{\mu_0} B - M \tag{2.6}$$

Now this equation can be simplified for linear, isotropic, nonmagnetic media as

$$D = \varepsilon_0 \varepsilon_r E \tag{2.7}$$

$$B = \mu_0 \mu_r H \tag{2.8}$$

where,

ε_0 is electric permittivity of vacuum in Farad per meter

μ_0 is the magnetic permeability of vacuum in Henry per meter

$\varepsilon_r$is the relative permittivity

$\mu_r$is the relative permeability

2.2 The EM or Electromagnetic Wave Equation

The EM wave equation which describes the field amplitude in time and space can be derived from Maxwell's equations. The wave equation can be derived by taking curl of Faraday's law

$$\nabla \times \nabla \times E = -\frac{\partial B}{\partial t} \tag{2.9}$$

or,

$$\nabla \times \nabla \times E = \nabla \times (-\mu \frac{\partial H}{\partial t}) \tag{2.10}$$

With the identities $\nabla \times \nabla \times E = \nabla(\nabla . E) - \nabla^2 E$ and $\nabla \times H = \varepsilon \frac{\partial E}{\partial t}$ we can simplify the above equation as

$$\nabla(\nabla . E) - \nabla^2 E = -\mu\varepsilon \frac{\partial^2 y}{\partial t^2} \tag{2.11}$$

From Gauss's law we can conclude that the divergence of E in a constant permittivity over space is zero. i,e $\nabla . E = 0$

Therefore, the final wave equation for electric field will be

$$\nabla^2 E - \mu\varepsilon \frac{\partial^2 E}{\partial t^2} = 0 \tag{2.12}$$

Similarly the wave equation for magnetic field can be derived as

$$\nabla^2 H - \mu\varepsilon \frac{\partial^2 H}{\partial t^2} = 0 \tag{2.13}$$

So, the general form of wave equation can be written as

$$\nabla^2 U - \frac{1}{v_p^2} (\frac{\partial^2 H}{\partial t^2}) = 0 \tag{2.14}$$

If the variation of the dielectric profile is negligible over distance, then we can write

$$\nabla^2 E - \frac{\varepsilon}{C^2} \frac{\partial^2 E}{\partial t^2} = 0 \tag{2.15}$$

Where $C = \frac{1}{\sqrt{\mu_0 \varepsilon_0}}$ velocity of light

The solution of wave equation is a harmonic function in time and space. Now if we assume this as a harmonic time dependence of the electric field,

$$E(r, t) = E(r) e^{-j\omega t} \tag{2.16}$$

Therefore, we get the Helmholtz equation

$$\nabla^2 E + K_0^2 \varepsilon E = 0 \tag{2.17}$$

where the vector of propagation $K_0 = \frac{\omega}{c}$, in free space

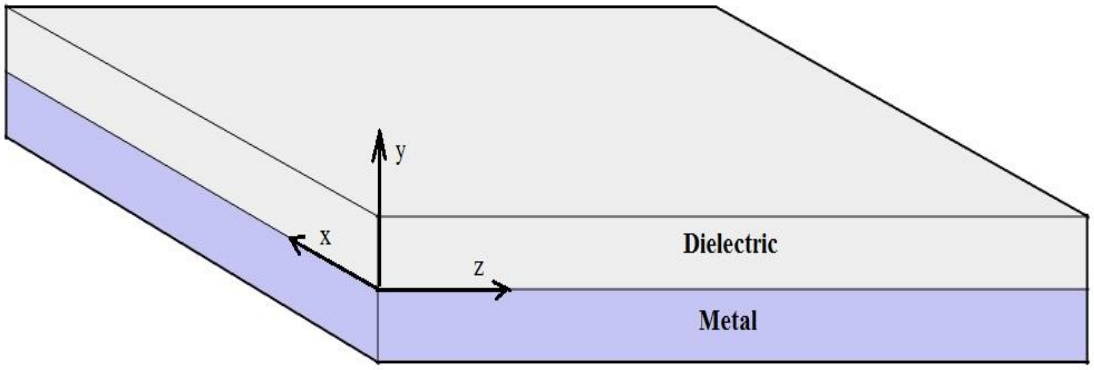

Fig 2.1: A Cartesian coordinate system at a metal dielectric interface

A typical planar waveguide geometry at a metal-dielectric interface is shown in fig 2.1. For simplicity let us assume that the propagation of the wave is along the x-direction of the Cartesian co-ordinate system and there is no spatial variation in y-direction. So, we can write

$$E(x, y, z) = E(z)e^{j\beta z} \tag{2.18}$$

Where $\beta = K_x$ which is call the propagation constant

Now inserting the value of E the wave equation will be

$$\frac{\partial^2 E(z)}{\partial z^2} + (K_0^2 \varepsilon - \beta^2)E = 0 \tag{2.19}$$

Similarly, we can derive the equation for the magnetic field H. The field E and H can be

decomposed in Cartesian co-ordinate system as

$$E = E_x.\vec{a}_x + E_y.\vec{a}_y + E_z.\vec{a}_z \tag{2.20}$$

$$H = H_x.\vec{a}_x + H_y.\vec{a}_y + H_z.\vec{a}_z \tag{2.21}$$

For Harmonic time dependence $\frac{\partial}{\partial t} = -j\omega$ and by solving the Ampere's law and Faraday's law, we get

$$\frac{\partial E_z}{\partial y} - \frac{\partial E_y}{\partial z} = j\omega\mu_0 H_x \tag{2.22}$$

$$\frac{\partial E_x}{\partial z} - \frac{\partial E_z}{\partial x} = j\omega\mu_0 H_y \tag{2.23}$$

$$\frac{\partial E_y}{\partial x} - \frac{\partial E_x}{\partial y} = j\omega\mu_0 H_z \tag{2.24}$$

$$\frac{\partial Hz}{\partial y} - \frac{\partial H_y}{\partial z} = j\omega\varepsilon_0 \varepsilon E_x \tag{2.25}$$

$$\frac{\partial Hx}{\partial z} - \frac{\partial H_z}{\partial x} = j\omega\varepsilon_0 \varepsilon E_y \tag{2.26}$$

$$\frac{\partial Hy}{\partial x} - \frac{\partial H_x}{\partial y} = j\omega\varepsilon_0 \varepsilon E_z \tag{2.27}$$

As the propagation is in x-direction in the form of $e^{j\beta x}$ which follows $\frac{\partial}{\partial x} = -j\beta$.

The homogeneity in y- direction makes $\frac{\partial}{\partial y} = 0$. So, the equation will be simplified as

$$-\frac{\partial E_y}{\partial z} = j\omega\mu_0 H_x \tag{2.28}$$

$$\frac{\partial E_x}{\partial z} - j\beta E_z = j\omega\mu_0 H_y \tag{2.29}$$

$$j\beta E_y = j\omega\mu_0 H_z \tag{2.30}$$

$$\frac{\partial H_y}{\partial z} = j\omega\varepsilon_0 \varepsilon E_x \tag{2.31}$$

$$\frac{\partial Hx}{\partial z} - j\beta H_z = j\omega\varepsilon_0 \varepsilon E_y \tag{2.32}$$

$$j\beta H_y = j\omega\varepsilon_0 \varepsilon E_z \tag{2.33}$$

The solution of the above equation can be characterized by two sets of solution with the polarized characteristics which are, Transverse Magnetic (TM) modes and Transverse Electric (TE) modes. The equations belong to TM modes are

$$E_x = -j\frac{1}{\omega\varepsilon_0\,\varepsilon}\frac{\partial H_y}{\partial z} \tag{2.34}$$

$$E_z = -\beta\frac{1}{\omega\varepsilon_0\,\varepsilon}H_y \tag{2.35}$$

Therefore, the wave equation for TM Polarized wave will be

$$\frac{\partial^2 H_y}{\partial z^2} + (K_0^2\varepsilon - \beta^2)H_y = 0 \tag{2.36}$$

Similarly, the TE polarized equations will be

$$H_x = j\frac{1}{\omega\mu_0}\frac{\partial E_y}{\partial z} \tag{2.37}$$

$$H_z = \beta\frac{1}{\omega\mu_0}E_y \tag{2.38}$$

And the corresponding TE wave equation will be

$$\frac{\partial^2 E_y}{\partial z^2} + (K_0^2\varepsilon - \beta^2)E_y = 0 \tag{2.39}$$

2.3 SPP at Single Interface

The simplest configuration of SPP propagation is at a single interface, that is in between a dielectric, having a positive dielectric constant ε_2 and a metal, having a negative dielectric constant ε_1. This is shown in fig 2.2. For metal the bulk plasmon frquency will be ω_p and the amplitude decays perpendicular to the $z-$ direction.

For the TM solutions in both spaces: metal and dielectric will be for $z > 0$

$$H_z(z) = A_2 e^{j\beta x} e^{-k_2 z} \tag{2.40}$$

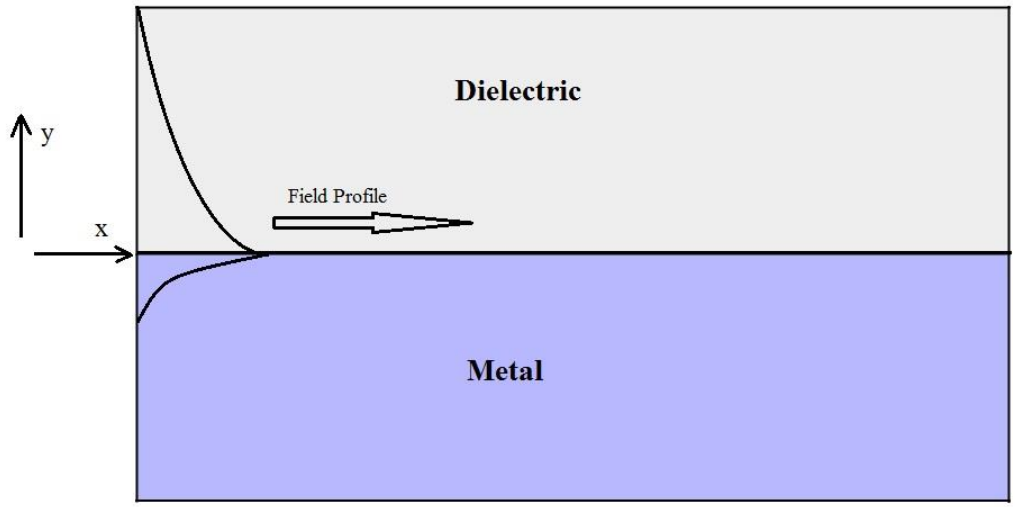

Fig 2.2: SPP at the Single interface.

$$E_x(z) = jA_2 \frac{1}{\omega\varepsilon_0\, \varepsilon_2} k_2 e^{j\beta x} e^{-k_2 z} \tag{2.41}$$

$$E_z(z) = -A_1 \frac{\beta}{\omega\varepsilon_0\, \varepsilon_2} e^{j\beta x} e^{-k_2 z} \tag{2.42}$$

And for $z < 0$

$$H_y(z) = A_1 e^{j\beta x} e^{k_1 z} \tag{2.43}$$

$$E_x(z) = -jA_1 \frac{1}{\omega\varepsilon_0\, \varepsilon_1} k_1 e^{j\beta x} e^{k_1 z} \tag{2.44}$$

$$E_x(z) = -A_1 \frac{\beta}{\omega\varepsilon_0\, \varepsilon_1} e^{j\beta x} e^{-k_1 z} \tag{2.45}$$

The continuity of H_y and $\varepsilon_i E_z$ at the metal dielectric interface gives $A_1 = A_2$ and

$$\frac{k_2}{k_1} = -\frac{\varepsilon_2}{\varepsilon_1} \tag{2.46}$$

The surface wave exists at the metal dielectric interface with opposite sign of their real dielectric permittivities. So, we can write

$$k_1^2 \varepsilon = \beta^2 - k_0^2 \varepsilon_1 \tag{2.47}$$

$$k_2^2\varepsilon = \beta^2 - k_0^2\varepsilon_2 \tag{2.48}$$

The dispersion relation of SPPs propagation can be found as

$$\beta = k_0\sqrt{\frac{\varepsilon_1\varepsilon_2}{\varepsilon_1+\varepsilon_2}} \tag{2.49}$$

The TE surface modes can be expressed as

$$E_y(z) = A_2 e^{j\beta x} e^{-k_2 z} \tag{2.50}$$

$$H_x(z) = -jA_2\frac{\beta}{\omega\mu_0}k_2 e^{j\beta x} e^{-k_2 z} \tag{2.51}$$

$$H_z(z) = -A_2\frac{\beta}{\omega\mu_0}k_2 e^{j\beta x} e^{-k_2 z} \tag{2.52}$$

for $z > 0$, and

$$E_y(z) = A_1 e^{j\beta x} e^{-k_1 z} \tag{2.53}$$

$$H_x(z) = jA_1\frac{\beta}{\omega\varepsilon_0\,\varepsilon_1}k_1 e^{j\beta x} e^{k_1 z} \tag{2.54}$$

$$H_z(z) = A_1\frac{\beta}{\omega\varepsilon_0\,\varepsilon_1}k_2 e^{j\beta x} e^{k_1 z} \tag{2.55}$$

for $z < 0$. The continuity of E_y and H_x requires

$$A_1\,(k_1 + k_2) = 0 \tag{2.56}$$

The surface requires that the real part of k_1 and k_2 should be greater than zero for confinement. This will be satisfied if $A_1 = A_2 = 0$. Therefore, there atr no surface modes for the TE polarization. SPP only exists for TM mode polarization.

2.4 SPP at Double Interface

Two mostly used double interface configurations of SPP waveguides are: Metal-Dielectric-Metal (MDM) and Dielectric-Metal-Dielectric (DMD). In these cases, SPPs are formed on both interfaces. When the distance is shorter than decay distance, it forms coupled mode of SPP. This coupled mode of propagation can also be sub-divided into even and odd modes, as shown in fig. 2.3.

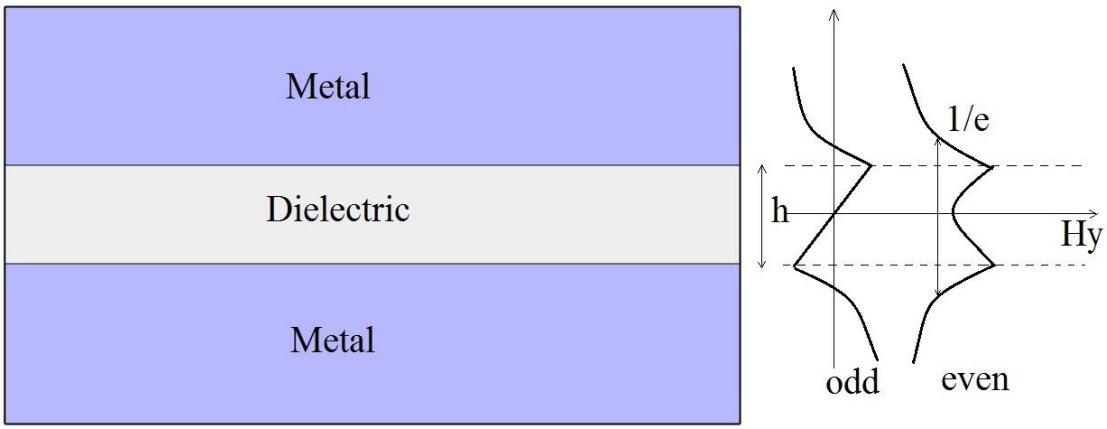

Fig 2.3: SPP at the double interface.

Chapter 3

Material Modelling Within Optical Range

3.1 Introduction

At low frequencies or for long wavelengths metals act as perfect conductors. Since they have zero field, they do not show any dispersive behavior. But at higher frequencies such as optical range metals behave as dispersive materials which means that there exists field inside metals. And for the frequencies higher than optical range metals act as dielectrics. Properties of SPPs depend highly on the material response to light. In this chapter we will be studying about the materials supporting SPP, descriptions and derivations of different models for describing the behavior of metal in the presence of light.

Now in the presence of an external oscillating electromagnetic field, three vectors can determine the behavior of any material. Such as, D (electrical flux density), E (electric field intensity) and P (polarization density). In the frequency domain the corresponding equations will be,

$$D(\omega) = \varepsilon(\omega)E(\omega) \tag{3.1}$$

$$P(\omega) = \varepsilon_0\chi(\omega)E(\omega) \tag{3.2}$$

$$D(\omega) = \varepsilon_0 E(\omega) + P(\omega) \tag{3.3}$$

Combining these two equations we get,

$$D(\omega) = \varepsilon_0 E(\omega)(1 + \chi(\omega)) \tag{3.4}$$

Where χ is the electric susceptibility which measures how easily it is polarized in response

to an applied electric field, and it is a dimensionless quantity.

Finally, the relation between the permittivity and susceptibility is

$$\varepsilon(\omega) = \varepsilon_0(1 + \chi(\omega)) \tag{3.5}$$

So, the relative permittivity will be

$$\varepsilon_r(\omega) = 1 + \chi(\omega) \tag{3.6}$$

For linear isotropic materials such as glass the above values become simple. But for a dispersive material, the frequency dependent permittivity and susceptibility should be modeled perfectly for getting the perfect response of the material for certain electromagnetic excitation. Some widely used material models are Drude model, Lorentz model and Lorentz-Drude model.

3.2 Different Material Models

3.2.1 The Drude Model

The Drude model of electrical conduction was first developed by Paul Drude. In his model he described the metal as a volume filled with stationary positive ions, immersed in a gas of electrons following the kinetic theory of gases. These electrons are free to move inside the metal without any interaction with each other. The electrons in a metal are subjected to two forces,

1. Driving force F_d
2. Damping force F_g

The driving force and the damping force can be expressed as

$$F_d = qE = -eE \tag{3.7}$$

$$F_g = -\Gamma v \tag{3.8}$$

As the two forces are opposite to each other, the resultant force will be

$$F = F_d - F_g \tag{3.9}$$

From Newton's first law of motion we can write

$$mr'' = -eE + \Gamma r' \tag{3.10}$$

where,

m is the mass of an electron
Γ is the damping constant in Newton second per meter

r is the displacement in meter.

v is the velocity of the electron .

q is the electrons charge.

The prime indicates differentiation order with respect to time

For time harmonic electric field and time harmonic displacement the equation will be,

$$E(t) = E_0 e^{-j\omega t} \Leftrightarrow E(\omega) \tag{3.11}$$
$$r(t) = R_0 e^{-j\omega t} \Leftrightarrow R(\omega) \tag{3.12}$$

From equation 3.10 the frequency domain form will be

$$mR''(\omega) - \Gamma mR'(\omega) + eE(\omega) = 0 \tag{3.13}$$

The derivatives of frequency domain will give

$$-m\omega^2 R''(\omega) + j\omega\Gamma mR'(\omega) + eE(\omega) = 0 \tag{3.14}$$

Simplifying the above equation, the displacement R will give

$$R(\omega) = \frac{-e}{m(j\Gamma\omega - \omega^2)} E(\omega) \tag{3.15}$$

The polarization for *n* number of electrons will be

$$P(\omega) = -neR(\omega) \tag{3.16}$$

Or,

$$P(\omega) = \frac{e^2 n}{m(j\Gamma\omega - \omega^2)} E(\omega) \tag{3.17}$$

An expression for the susceptibility can also be obtained from the above equation and that will be

$$\frac{P(\omega)}{\varepsilon_0 E(\omega)} = \frac{e^2 n}{\varepsilon_0 m(j\Gamma\omega - \omega^2)} = \chi(\omega) \tag{3.18}$$

Now substituting this value in equation 3.6 we get

$$\varepsilon_r(\omega) = 1 + \frac{e^2 n}{\varepsilon_0 m(j\Gamma\omega - \omega^2)} \tag{3.19}$$

if we consider ω_p as the plasma frequency that will provide

$$\omega_p^2 = \frac{e^2 n}{\varepsilon_0 m} \tag{3.20}$$

So, the frequency dependent flux density will be

$$D(\omega) = \varepsilon_0 (1 + \frac{\omega_p^2}{(j\Gamma\omega - \omega^2)}) E(\omega) \tag{3.21}$$

For low frequency, the term $\Gamma\omega \ll 1$. Therefore, the dispersive relation can be reduced to

$$D(\omega) = \varepsilon_0 (1 - \frac{\omega_p^2}{(\omega^2)}) E(\omega) \tag{3.22}$$

3.2.2 The Lorentz Model

The Lorentz model gives a simpler picture of the atom, as shown in fig 3.1. The model is a very useful tool to visualize atom-field interaction. In this model, Lorentz modeled an atom as a mass (nucleus) connected to another smaller mass (electron). However, electrons in the Lorentz model do not move freely inside the metal instead, they are bound to atoms. So, there is a restoring force acting between them which can be denoted by F_r.

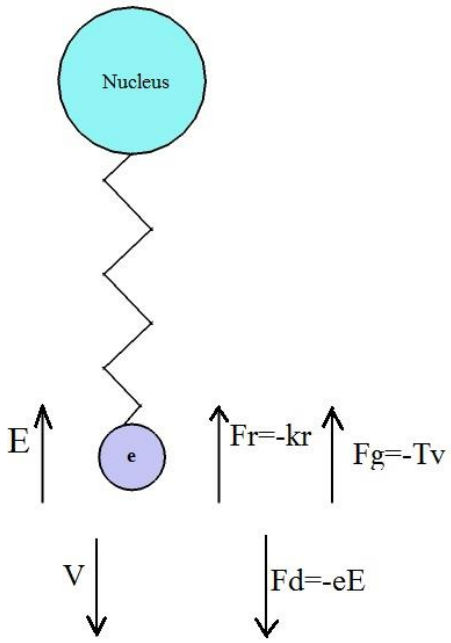

Fig 3.1: Lorentz model

The restoring force can be written as

$$F_r = -kr \tag{3.22}$$

where *k* is the spring constant in Newtons per meter.

Similarly from the law of motion we can say that

$$mr'' + \Gamma mr'(\omega) + mkr + eE = 0 \tag{3.23}$$

In frequency domain the above equation will be

$$R(\omega)(m\omega_0^2 + j\omega\Gamma m - m\omega^2 - eE(\omega) = 0 \tag{3.24}$$

Considering the natural frequency $\omega_0 = \sqrt{\frac{k}{m}}$ we get

$$R(\omega) = \frac{-e}{m(\omega_0^2 + j\omega\Gamma - \omega^2)} E(\omega) \tag{3.25}$$

Therefore the susceptibility can be found as

$$\frac{P(\omega)}{\varepsilon_0 E(\omega)} = \frac{e^2 n}{\varepsilon_0 m(\omega_0^2 + j\omega\Gamma - \omega^2)} = \chi(\omega) \tag{3.26}$$

So from the equation 3.4 the expression for D can be expressed in frequency domain as

$$D(\omega) = \varepsilon_0(1 + \frac{\omega_p^2}{\omega_0^2 + j\omega\Gamma - \omega^2})E(\omega) \tag{3.27}$$

3.2.3 The Lorentz-Drude Model

In the Lorentz-Drude (LD) model, which is the most general form when an EM field is applied to a metal, the electrons of two types oscillate inside the metal, and they contribute to the permittivity. The free electrons contribute a permittivity of the Drude model, and the bound electrons contribute a permittivity of the Lorentz model. The permittivity in the LD model is given by

$$\varepsilon = \varepsilon_{free} + \varepsilon_{bound} \tag{3.29}$$

Where

$$\varepsilon_{free} = 1 + \frac{\omega_p}{(j\Gamma\omega - \omega^2)} \tag{3.30}$$

$$\varepsilon_{bound} = \frac{\omega_p}{\omega_0 + j\omega\Gamma - \omega^2} \tag{3.31}$$

Therefore combining both the model together the electric field density D in fre-quency domain will be

$$D(\omega) = \varepsilon_0(1 + \frac{\omega_p}{j\Gamma\omega - \omega^2} + \frac{\omega_p^2}{\omega_0^2 + j\omega\Gamma - \omega^2})E(\omega) \tag{3.32}$$

The above relation is known as the Lorentz-Drude model.

3.3 Material Dispersion

Dispersion can be defined as the variation of the propagating waves wavelength with frequency. It is also sometimes defined as the variation of propagating waves wave number $k = \frac{2\pi}{\lambda}$ with angular frequency $\omega = 2\pi f$. So the one dimensional wave equation will be

$$\frac{\partial^2 u}{\partial t^2} = v^2 \frac{\partial^2 u}{\partial x^2} \tag{3.47}$$

Where,

$$v^2 = \frac{1}{\varepsilon\mu}$$

The solution of the above wave equation can be written in phasor form as

$$u(x,t) = e^{j(\omega t - kx)} \tag{3.48}$$

Now putting this value in the wave equation we get

$$(j\omega)^2 e^{j(\omega t - kx)} = v^2(-jk)^2 e^{j(\omega t - kx)} \tag{3.49}$$

Finally from this equation we get

$$k = \pm\frac{\omega}{v} \tag{3.50}$$

The + sign is for -x directed wave propagation and - sign is for +x directed wave propagation. The magnetic flux density and electric flux density for dispersive medium are-

$$D(\omega) = \varepsilon(\omega)E \tag{3.51}$$

$$B(\omega) = \mu(\omega)H \tag{3.52}$$

Here both $\varepsilon(\omega)$ and $\mu(\omega)$ are frequency dependent functions.

Chapter 4

Overview of Finite-Difference Time-Domain Method

4.1 The Yee Algorithm

The algorithm used in FDTD simulations is known as the Yee algorithm. The original proposal was intended for homogeneous, isotropic and lossless media based on discretizing the volume into cells in Cartesian coordinates. The Yee algorithm solves for both electric and magnetic fields using the coupled Maxwell's time-dependent curl equations, rather than solving for the electric field alone (or the magnetic field alone) with a wave equation.

The method begins with two of Maxwell's equations:

$$D\frac{\partial \vec{H}}{\partial t} = -\frac{1}{\mu}\nabla \times \vec{E} \tag{4.1}$$

$$D\frac{\partial \vec{E}}{\partial t} = \frac{1}{\varepsilon}\nabla \times \vec{H} \tag{4.2}$$

The electric and magnetic fields are three dimensional vectors. Each equation can be converted into three coupled scalar first order differential equations. The derivatives are both in space and time. The curl operations of equations 4.1 and equation 4.2 yields the following six equations in Cartesian coordinates

$$\frac{\partial E_z}{\partial y} - \frac{\partial E_y}{\partial z} = \mu\frac{\partial H_x}{\partial t} \tag{4.3}$$

$$\frac{\partial E_x}{\partial z} - \frac{\partial E_z}{\partial x} = \mu\frac{\partial H_z}{\partial t} \tag{4.4}$$

$$\frac{\partial E_y}{\partial x} - \frac{\partial E_x}{\partial y} = \mu\frac{\partial H_z}{\partial t} \tag{4.5}$$

$$\frac{\partial Hz}{\partial y} - \frac{\partial H_y}{\partial z} = \varepsilon \frac{\partial E_x}{\partial t} \tag{4.6}$$

$$\frac{\partial Hx}{\partial z} - \frac{\partial H_z}{\partial x} = \varepsilon \frac{\partial E_y}{\partial t} \tag{4.7}$$

$$\frac{\partial Hy}{\partial x} - \frac{\partial H_x}{\partial y} = \varepsilon \frac{\partial E_z}{\partial t} \tag{4.8}$$

Then the scalar differential equations are converted into difference equations. In order to do that, discretization is required for both space and time. For space discretization, Yee visualized the field components arranged within a unit cell (voxel). The electric field components are stored on the corresponding cell edges, while the magnetic field components are stored on the corresponding face centers. The fields are located in a way where each *E* component is surrounded by four

H components and vice versa, which leads to a spatially coupled system of field circulations corresponding to the law of Faraday and Ampere. The figure 4.1 shows the Yee's spatial grid.

Considering a two dimensional TM (Transverse Magnetic) polarized field case,

$$\frac{\partial E_x}{\partial t} = \frac{1}{\varepsilon} \frac{\partial H_z}{\partial y} \tag{4.9}$$

$$\frac{\partial E_y}{\partial t} = \frac{1}{\varepsilon} \frac{\partial H_z}{\partial x} \tag{4.10}$$

$$\frac{\partial H_z}{\partial t} = \frac{1}{\mu} \left(\frac{\partial E_x}{\partial y} - \frac{\partial E_y}{\partial x} \right) \tag{4.11}$$

Central difference approximation is applied in each of the equations 4.9, 4.10 and 4.11 which finally conclude in a spatial scalar difference equations in 4.12, 4.13 and 4.14.

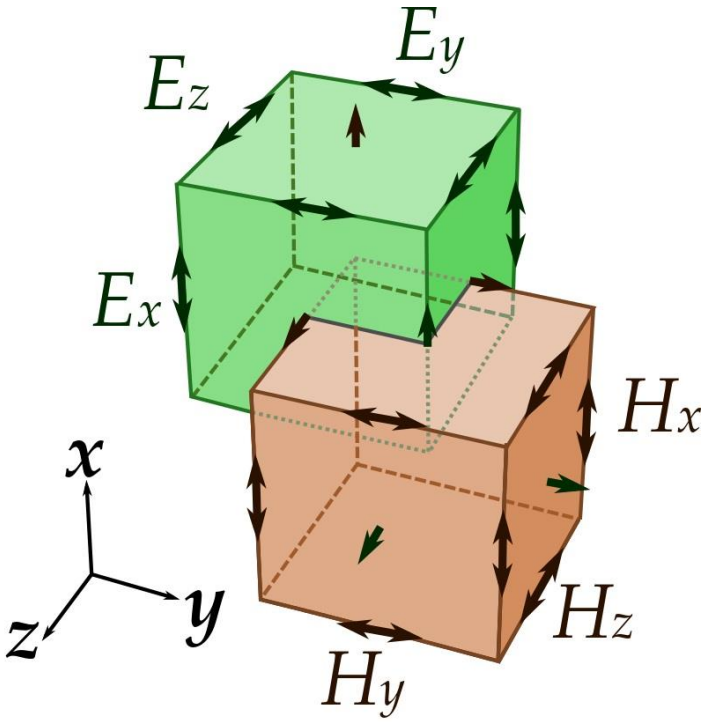

Fig 4.1: Yee's spatial grid.

$$\frac{\partial E_x}{\partial t} = \frac{1}{\varepsilon}\frac{H_z(i,j)-H_z(i,j-1)}{\Delta y} \tag{4.12}$$

$$\frac{\partial E_y}{\partial t} = \frac{1}{\varepsilon}\frac{H_z(i,j)-H_z(i-1,j)}{\Delta x} \tag{4.13}$$

$$\frac{\partial H_z}{\partial t} = \frac{1}{\mu}\left(\frac{E_x(i,j+1)-E_x(i,j)}{\Delta y} - \frac{E_y(i+1,j)-E_y(i-1,j)}{\Delta x}\right) \tag{4.14}$$

In order to consider the time derivatives, the time axis is to be considered as shown in the figure. The electric and magnetic field are mapped half a step apart along the time axis. Again applying the central difference approximation, the equations 4.12, 4.13 and 4.14 become:

$$\frac{E_x^{n+1}\left(i+\frac{1}{2},j\right)-E_x^{n}(i+\frac{1}{2},j)}{\Delta t} = \frac{1}{\varepsilon}\frac{H_z^{n+\frac{1}{2}}\left(i+\frac{1}{2},j\right)-H_z^{n+\frac{1}{2}}(i+\frac{1}{2},j-\frac{1}{2})}{\Delta y}$$

$$\frac{E_y^{n+1}\left(i,j+\frac{1}{2}\right)-E_y^{n}(i,j+\frac{1}{2})}{\Delta t}=-\frac{1}{\varepsilon}\frac{H_z^{n+\frac{1}{2}}\left(i+\frac{1}{2},j+\frac{1}{2}\right)-H_z^{n+\frac{1}{2}}(i-\frac{1}{2},j+\frac{1}{2})}{\Delta y}$$

$$\frac{H_z^{n+\frac{1}{2}}\left(i+\frac{1}{2},j+\frac{1}{2}\right)-H_z^{n-\frac{1}{2}}(i+\frac{1}{2},j+\frac{1}{2})}{\Delta t}=-\frac{1}{\mu}\left(\frac{E_x^{n+1}\left(i+\frac{1}{2},j+1\right)-E_x^{n}(i+\frac{1}{2},j)}{\Delta y}-\frac{E_y^{n}\left(i+1,j+\frac{1}{2}\right)-E_y^{n}(i,j+\frac{1}{2})}{\Delta x}\right)$$

Each field component depends on the field of previous time step itself and the surrounding component in Yee's algorithm.

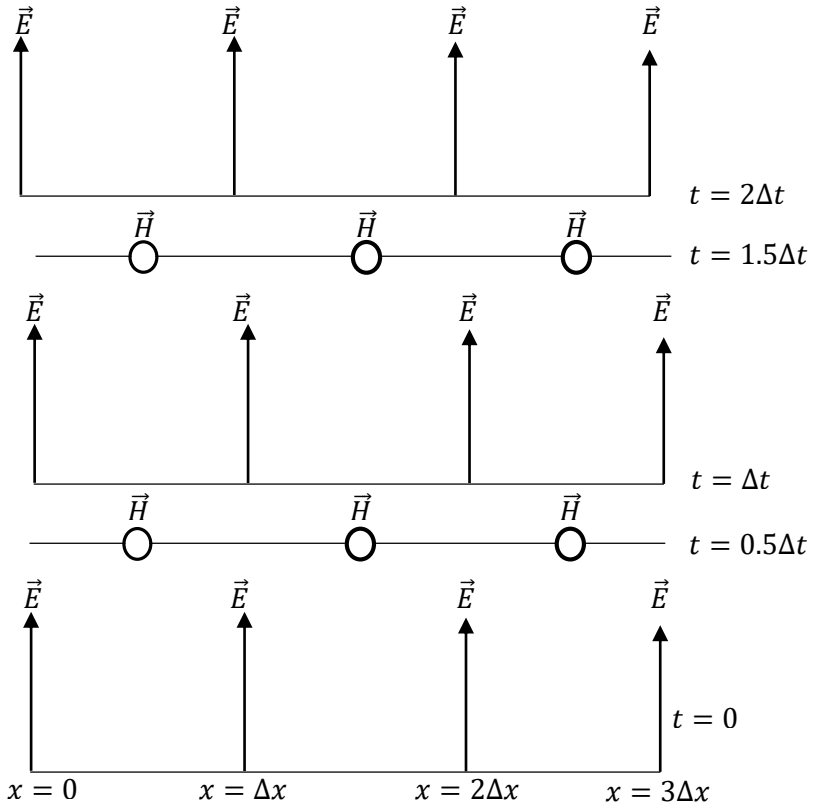

Fig 4.2: The temporal scheme of FDTD method.

Numerical stability of the Yee algorithm is required to be ensured. In an unstable algorithm the computed magnitude of electric and magnetic field components will gradually increase without limit with the progression of simulation. To guarantee numerical stability, the EM field's propagation should not be faster than the al-lowed limit which is imposed by the phase velocity within the material. This is done by

limiting time step Δt using the Courant-Friedrichs-Lewy criterion for the general Yee FDTD grid as follows:

$$\Delta t \leq \left\{ \frac{1}{v_p \sqrt{\frac{1}{(\Delta x)^2}+\frac{1}{(\Delta y)^2}+\frac{1}{(\Delta z)^2}}} \right\} \tag{4.15}$$

where Δx, Δy and Δz indicate the spatial Cartesian grid increments.

4.1 Absorbing Boundary Condition (ABC)

In FDTD method, a space of theoretically infinite extent with a finite computational cell is simulated due to limited computer resources. The boundary is said to be ideally absorbing, without any non-physical reflection back to the region. To accomplish this, a number of boundary conditions such as Berenger's perfectly matched layer (PML), have been proposed. An artificial layer surrounds the computational domain so that most of the outgoing waves are absorbed. The electromagnetic fields are made to attenuate rapidly until they become equal to zero, so that they do not produce any reflections.

4.2 Material Dispersion in FDTD

The material is said to be dispersive when the permittivity and permeability of a material are functions of frequency. In reality the assumption of constant relative permittivity is not absolutely correct. Because by doing so, instantaneous polarization of charge within a material is being assumed. In order to exploit the realistic wave propagation, dispersive FDTD techniques become necessary. The existing FDTD based algorithms for the analysis of material dispersion can be categorized into three types:

1) the auxiliary differential equation (ADE),
2) the Z-transform methods, and
3) methods based on discrete convolution of the dispersion relation or the recursive

convolution (RC) method [38].

We will highlight on the ADE dispersive FDTD method as we have applied in material modeling. The other methods will also be briefly discussed.

4.2.1 The Auxiliary Differential Equation (ADE)

Taflove introduced the auxiliary differential equation to the FDTD modeling in order to integrate the dispersion relation into the model. The dispersion relation is converted from frequency domain to time domain through Fourier transform in the basic step of the procedure. The Fourier transform results in a relationship between the new *E* field value and the previous *E* and *D* values, which can be added to the algorithm to update the *E* fields. The new algorithm with ADE becomes

$$\frac{\partial}{\partial t}H_z = -\frac{1}{\mu}\left(\frac{\partial E_x}{\partial y} - \frac{\partial E_y}{\partial x}\right) \tag{4.16}$$

$$\frac{\partial}{\partial t}D_x = \frac{\partial H_z}{\partial y} \tag{4.17}$$

In order to get the function relating *D* to *E* in a dispersive medium, we start with

$$D(\omega) = \varepsilon_0 \frac{\sigma}{j\omega} E(\omega) \tag{4.18}$$

Multiplying by $j\omega$

$$j\omega D(\omega) = \varepsilon_0 \sigma E(\omega) \tag{4.19}$$

Applying the Fourier transform in equation 4.19

$$\frac{d}{dt}D(t) = \varepsilon_0 \sigma E(t) \tag{4.20}$$

Discretizing equation 4.20 equation using forward difference method

$$\frac{D^n - D^{n-1}}{\Delta t} = \varepsilon_0 \sigma E(t) \tag{4.21}$$

Finally solving for *E*, we find the update equation

$$E^n = \frac{D^n - D^{n-1}}{\varepsilon_0 \sigma \Delta t} \tag{4.22}$$

4.2.2 The Z-transform Methods

The Z-transform is a faster method compared to ADE method. Sullivan used the Z-transform method for the first time in order to introduce the dispersion relation into the FDTD algorithm.

The Z-transform of the equation

$$D(\omega) = \varepsilon(\omega) E(\omega) \tag{4.23}$$

is -

$$D(z) = \varepsilon(z) \Delta t E(z) \tag{4.24}$$

—

where $\varepsilon(z)$ is the z-transform of $\varepsilon(\omega)$ and is the sampling period. As already done in ODE, let us consider the material dispersion as $\frac{\sigma}{j\omega}$, the relation between *D* and *E* is given by

$$D(\omega) = \frac{\sigma \varepsilon_0}{1 - z^{-1}} \Delta t E(z) \tag{4.25}$$

Multiplying by $(1 - z^{-1})$, we find

$$D(z)(1 - z^{-1}) = \sigma \varepsilon_0 E(z) \tag{4.26}$$

Or,

$$D(z) - z^{-1} D(z) = \sigma \varepsilon_0 E(z) \tag{4.27}$$

Performing inverse z-transform

$$D^n - D^{n-1} = \sigma \varepsilon_0 \Delta t E^n \tag{4.28}$$

Finally, for solving E from equation 4.28, we find

$$E^n = \frac{D^n - D^{n-1}}{\sigma \varepsilon_0 \Delta t} \tag{4.29}$$

Which is same as the final update equation derived by ADE method.

4.3.3 Piecewise Linear Recursive Convolution Method

Luebbers et al. formulated the first frequency dispersive FDTD algorithm using the recursive convolution (RC) scheme. Later it became piecewise linear recursive convolution (PLRC) method [39]. Initially developed for Debye media, the approach was later extended for the study of wave propagation in a Drude material [40], N-th order dispersive media, an anisotropic magneto-active plasma, ferrite material and the bi-isotropic/chiral media [41] [42] [43].

The RC approach, typically being faster and having required fewer computer memory resources than other approaches, is usually less accurate. But in case of multiple pole mediums, it is easier to follow the RC approach.

In the initial derivation of PLRC method for a linear dispersive medium, the relation between electric flux density and electric field intensity is expressed as:

$$D(t) = \varepsilon_\infty \varepsilon_0 E(t) + \varepsilon_0 \int_0^t E(t-\tau)\chi(\tau)d\tau \tag{4.30}$$

which can be discretized as:

$$D^n = \varepsilon_\infty \varepsilon_0 E^n + \varepsilon_0 \int_0^{n\Delta t} E(n\Delta t - \tau)\chi(\tau)d\tau \tag{4.31}$$

The PRC method is further preceded from this basing discrete equation.

4.2.3 The General Algorithm

The derivation of equations for multi-pole dispersion relation is more difficult compared to the single pole-pair dispersion relation. For example, for six-pole Lorentz-Drude dispersion the required derivation process is lengthy. Additionally, the memory required for computation is also vast. There are various methods proposed by researchers regarding this topic such as Taflove's matrix inversion method, Multi-term dispersion by Okoniewski, etc. However Alsunaidi and Al-Jabr proposed a general algorithm technique which solves various problems regarding previous methods. The major advantage of this technique is that it requires only one algorithm for any dispersion relation. The dispersive relation has the general form as

$$D(\omega) = \varepsilon(\omega)E(\omega) \tag{4.32}$$

which can be expressed in terms of summation of poles

$$D(\omega) = \varepsilon_\infty \varepsilon_0 E(\omega) + \sum_i^N P_i(\omega) \tag{4.33}$$

where *N* is the number of poles. Applying Fourier transform, this equation becomes

$$D^{n+1} = \varepsilon_\infty \varepsilon_0 E^{n+1} + \sum_i^N P_i^{n+1} \tag{4.34}$$

or

$$E^{n+1} = \frac{D^{n+1} - \sum_i^N P_i^{n+1}}{\varepsilon_\infty \varepsilon_0} \tag{4.35}$$

This term P_i can be any form of dispersion relation such as the Debye, the Drude or just the conductivity term. This the final solved equation for *E*.

Chapter 5

Parameter Extraction of Optical Materials

The six-pole Lorentz-Drude model parameters for silver metal is presented. A nonlinear optimization algorithm has been developed in order to extract the parameters for the metals. The extracted parameters have been used to determine the complex relative permittivity of the metals in optical and near-IR region of electromagnetic spectrum. The obtained results have been compared with the experimental values and an excellent agreement has been found.

5.1 Material Models

5.1.1 Six-pole Lorentz-Drude model

5.1.1.1 Metals

The complex relative permittivity function of the six-pole Lorentz-Drude model is described by the following equation

$$\in_r(\omega) = \in_\infty + \frac{\omega_0^2(\in_s - \in_\infty)}{\omega_0^2 + j2\delta\omega - \omega^2} \tag{5.1}$$

where, ε_∞ is the infinite frequency relative permittivity, ε_S is the zero frequency relative permittivity, ω is the angular frequency, j is the imaginary unit, δ is the damping coefficient and $\boldsymbol{\omega_0}$ is the frequency of pole air.

From equation 5.1 we can see that the six-pole Lorentz-Drude model for metals can be described by four independent parameters which are ε_∞, ε_s, ω_0 and δ.These four parameters need to be optimized in order to model metals.

5.1.2 Single-pole Lorentz model

5.1.2.1 Dielectrics

The frequency dependent permittivity function of Single-pole Lorentz Model is given by,

$$\epsilon_r(\omega) = 1 - \frac{f_o\omega_p^2}{\omega^2 - j\mathrm{T}_o\omega} + \sum_{i=1}^{5} \frac{f_i\omega_p^2}{\omega_i^2 + j\mathrm{T}_i\omega - \omega^2} \quad (5.2)$$

.

5.1.3 Developing the Simulation Model

The simulation model we have developed is based on the FDTD method. We have utilized the general auxiliary differential equation (ADE) based FDTD approach in order to incorporate the frequency dependent dispersion property of the constituent materials. This algorithm is useful for the simulation of materials with different dispersive properties. The perfectly matched layer has been integrated at all the boundaries in order to prevent back reflections.

Considering the material dispersion, the frequency-dependent electric flux density can be given by-

$$D(\omega) = \epsilon_o\epsilon_\infty E(\omega) + P(\omega). \quad (5.6)$$

The general Lorentz model for polarization (ω) is given by-

$$P(\omega) = \frac{a}{b + jc\omega - \mathrm{d}\omega^2} E(\omega)\,, \quad (5.7)$$

By inverse Fourier transform, it can be written in time domain as-

. $$bP(t) + cP'(t) + dP''(t) = aE(t) \quad (5.8)$$

Now, turning to FDTD scheme, above equation can be presented as-

$$P^{n+1} = C_1 P^n + C_2 P^{n-1} + C_3 E^n. \quad (5.9)$$

Where, $C_1 = \frac{4d-2b\Delta t^2}{2d+c\Delta t}$, $C_2 = \frac{-2d-c\Delta t}{2d+c\Delta t}$, and $C_3 = \frac{2a\Delta t^2}{2d+c\Delta t}$.

The values of C_1, C_2, C_3 depends on the material under consideration. Finally, equation of field intensity has the form-

$$E^{n+1} = \frac{D^{n+1} - \sum_{i=1}^{N} P_i^{n+1}}{\epsilon_o \epsilon_\infty} \quad (5.10)$$

Where N is the number of poles and D^{n+1} is the next value of electric flux density after one iteration in FDTD algorithm.

Chapter 6

Designing the Add-drop Ring Resonators

6.1 Introduction

6.1.1 Add-drop ring resonator

An add-drop or channel drop ring resonator has two access waveguides, as shown in figure 6.1. The second waveguide makes it possible to drop or add signals at the resonance wavelength to the signal in the input waveguide. Just like for an all-pass resonator, constructive interference builds up the power in the ring on resonance. Because a second waveguide is coupled to the micro-ring, part of this power couples to this waveguide and light at the resonance wavelength is dropped to the drop port, hence the name. The drop port will show transmission peaks at the resonance wavelengths. The output of the access waveguide, the through port, features a dip in transmitted power on resonance. Off resonance, the pass transmission is maximum and the drop port is dark.

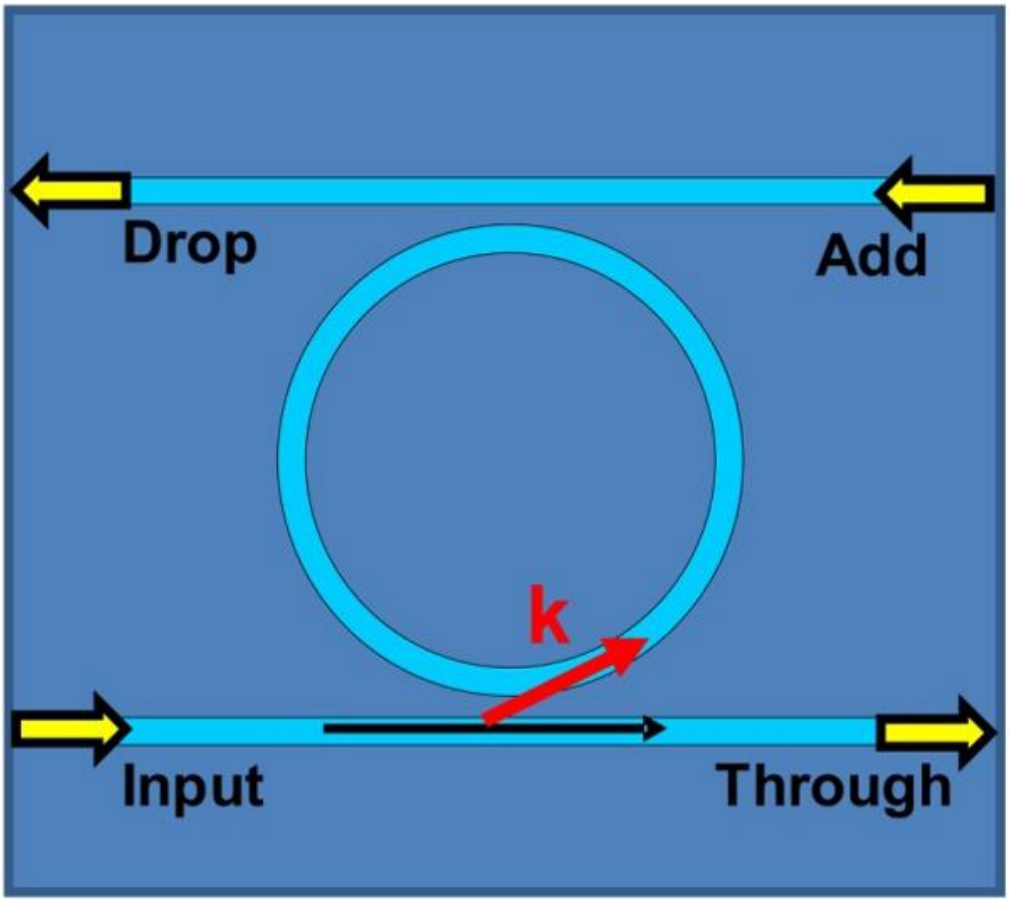

Fig 6.1: An add-drop ring resonator

The add-drop resonator is described by two transmission functions, one for the pass port and one for the drop port that are given by equation 5.10:

(5.11)

As an add-drop resonator has two directional coupler sections, two different amplitude self-coupling coefficients are featured in the equations. $r1$ represents the self-coupling of the input directional coupler and $r2$ is the self-coupling coefficient of the directional coupler leading to the drop port. The transmission spectra are plotted in figure 6.2.

When comparing the pass port transmission to that of an all-pass resonator, we see that the second coupler acts as an extra loss mechanism in the microring. The add-drop resonator is critically coupled if $r1 = ar2$. Like for an all-pass microring, the pass transmission of the add-drop resonator at critical coupling is zero, but the FWHM of the add-drop ring is larger because of the higher losses induced by the drop waveguide.

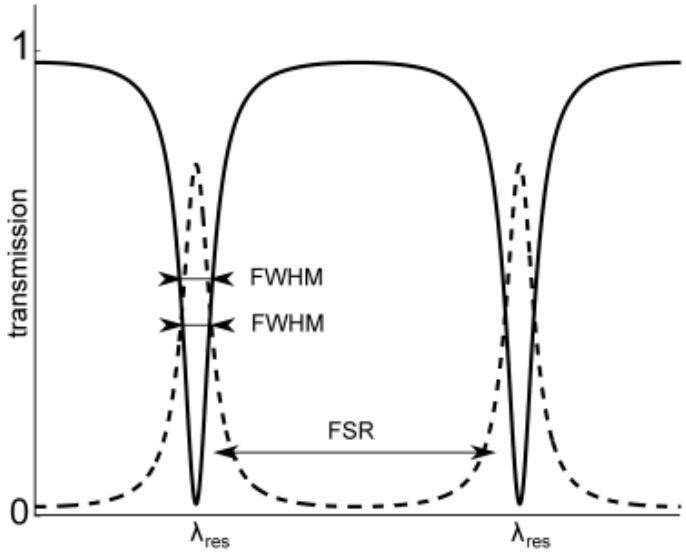

Fig 6.2: Transmission spectrum of a typical add-drop ring resonator configuration.

6.2 Add-drop ring resonator configurations

6.2.1 Basic configuration with a circular ring

The basic add-drop ring resonator consists of a circular ring surrounded by two straight dielectric waveguides on either side. In the structure designed here shown in Fig. 6.3, the gray area represents silver, which is the metal used in this case, and the white area represents air, which is the dielectric. The entire structure measures 1000nm by 1000nm and is made of silver, with the circular ring and the dielectric waveguides containing air. Thus, a metal-dielectric-metal interface is formed on either side of this ring, for the

propagation of the surface plasmon polariton (SPP) waves. The geometric parameters of the shape are as follows. The radius of the ring, r=150nm. The gap between the ring and the waveguides on either side, known as the coupling distance, d=5nm. The width of the waveguides and the ring, W=50nm, and this is kept constant for all the structures designed in this book.

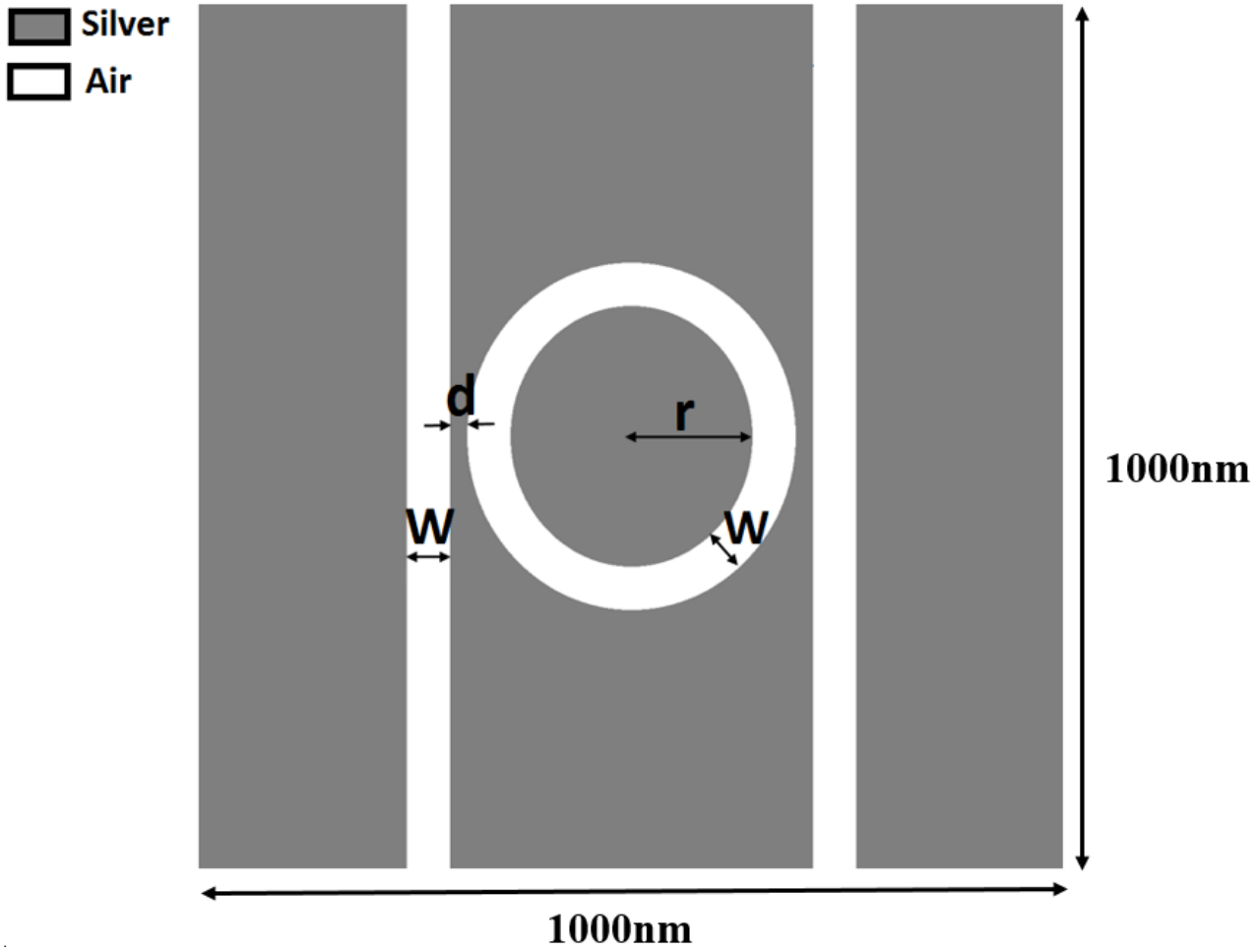

Fig 6.3: Circular add-drop ring resonator

6.2.2 Variations of the geometric shape of the ring

The shape of the ring in the add-drop configuration was varied to analyze and compare the difference in transmission characteristic from the basic circular ring. Figure 6.4 and 6.5 show two such variations. Both are elliptical structures, one with a vertical major axis, called a vertical major axis ellipse, and the other with a horizontal major axis, called a horizontal major axis ellipse. From the figures, it is seen that the main difference between these structures and the circular ring is the coupling length. The coupling length is the length of the ring that is in close proximity to the input waveguide. Simulations were carried out to observe the difference in transmission characteristics between these two sub-structures, and also with the circular ring. In both cases, the major axis length was kept at 660nm, and the minor axis length at 300nm. The coupling distance, d=5nm. The width of the ring and waveguides were kept constant at 50nm, as stated previously.

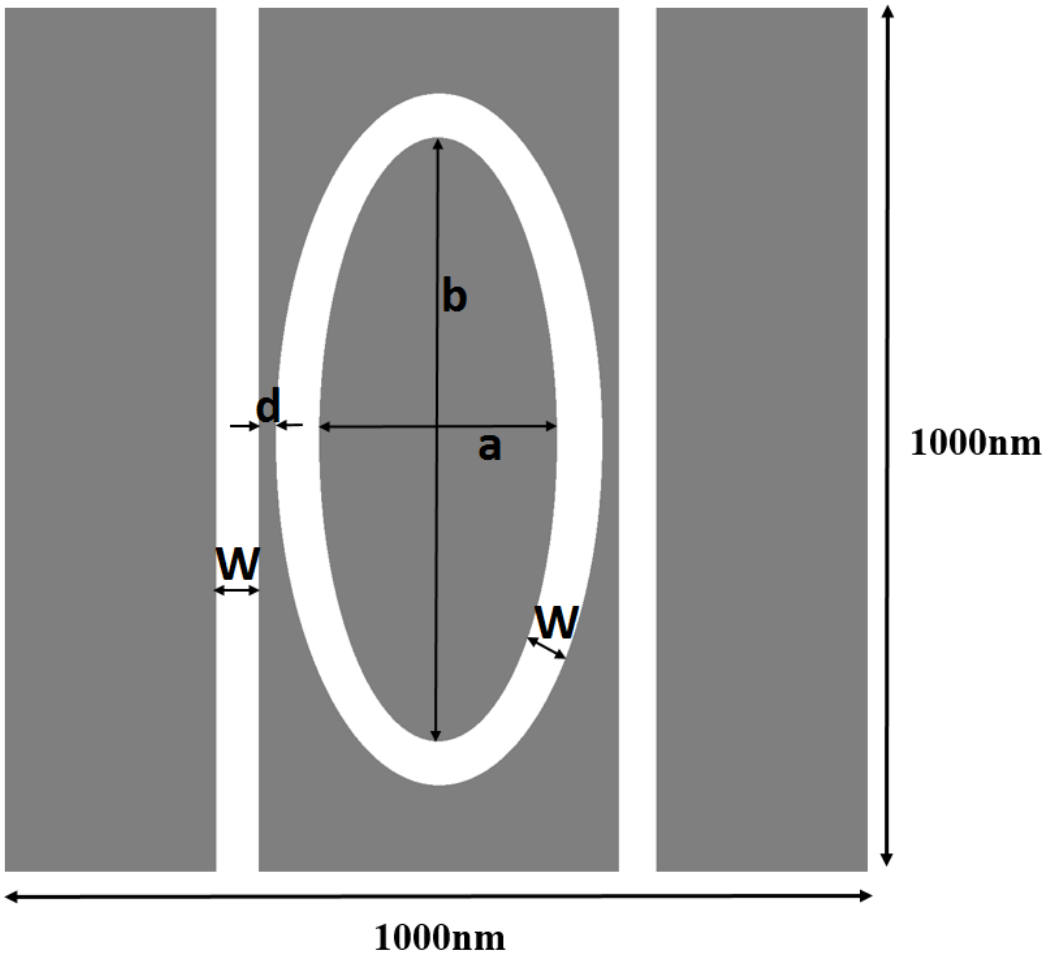

Fig 6.4: Vertical major axis elliptical ring configuration.

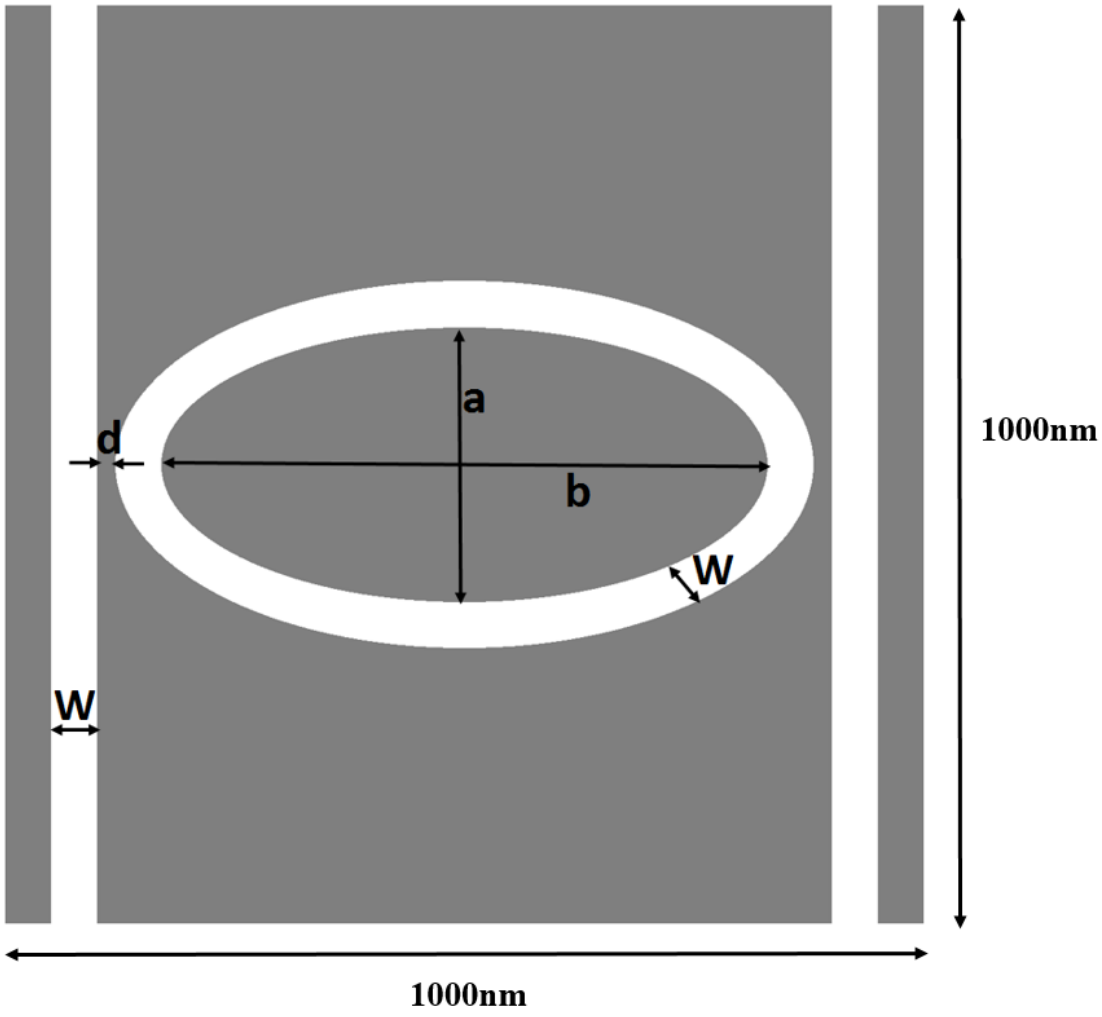

Fig 6.5: Horizontal major axis elliptical ring configuration

The next two structures consist of a normal square ring and a round-edge square ring, shown in Fig 6.6 and Fig 6.7 respectively. The length of the sides of each ring is, L=400nm. Here, the main difference between these two structures is the amount of bending at the corners. The bends at the corners of the round-edge square ring are less sharp compared to the normal square-ring. Simulations were run on these two structures to determine what effects the amount of bending has on the transmission characteristics.

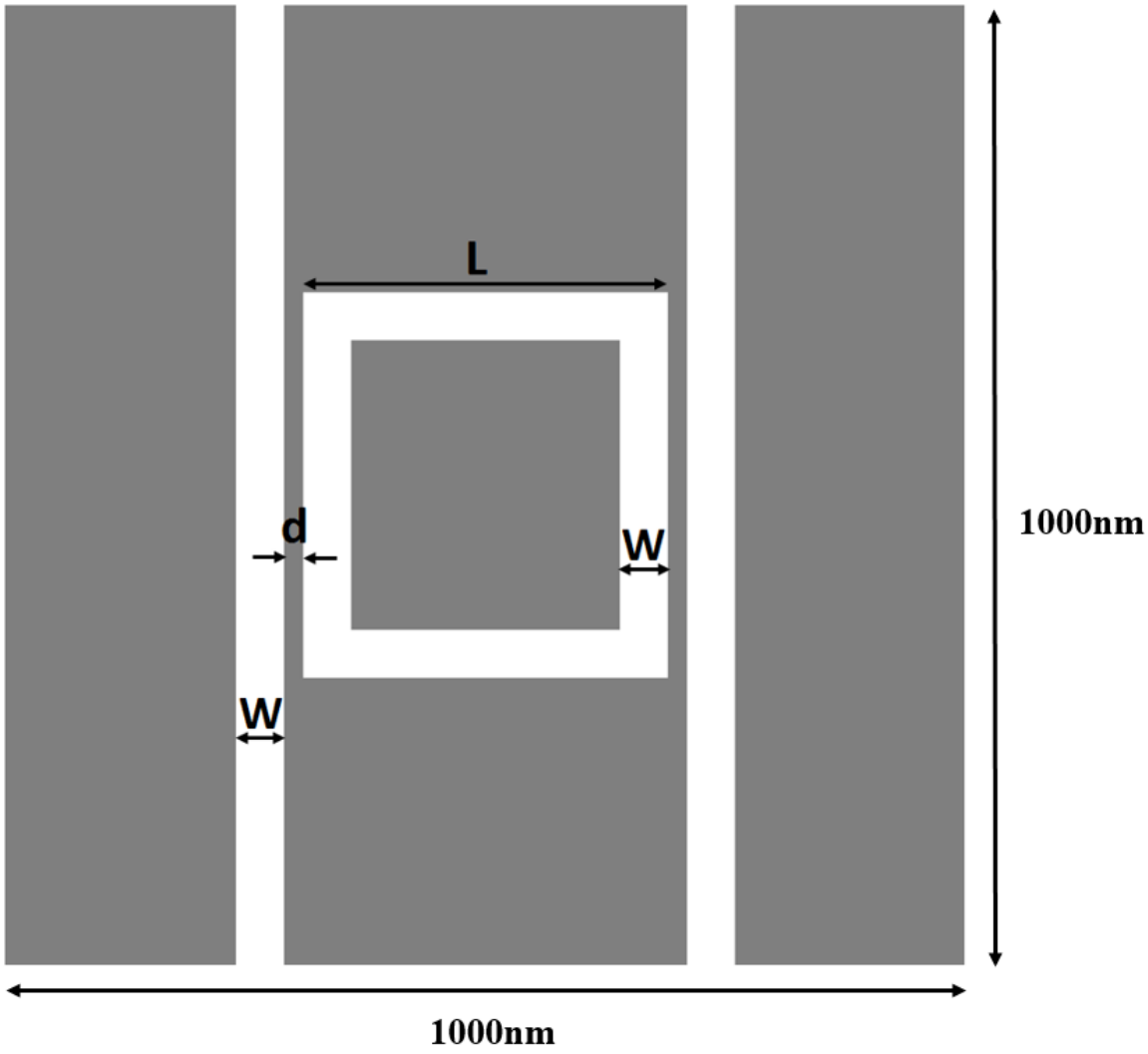

Fig 6.6: Square ring configuration

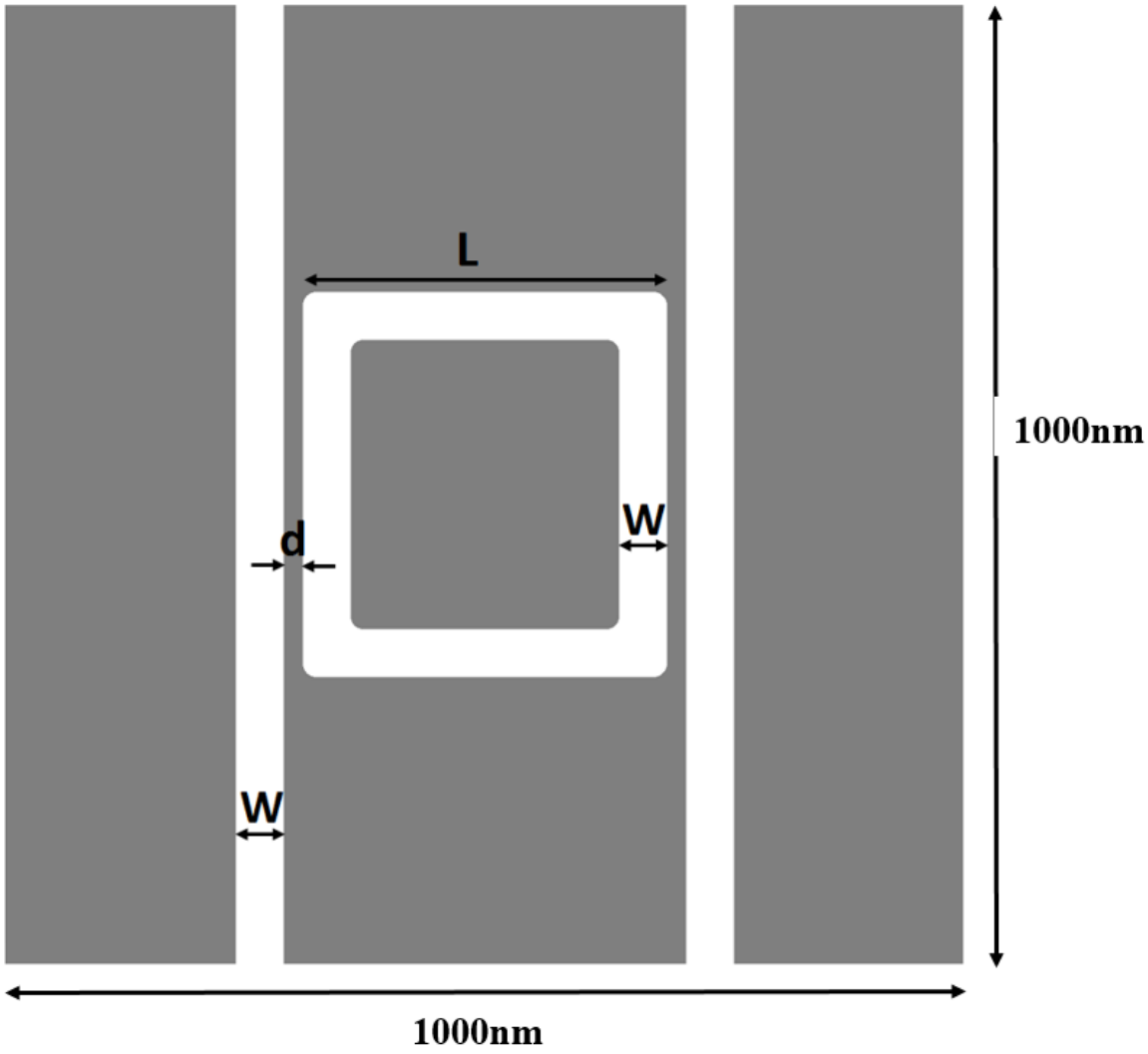

Fig 6.7: Round-edge square configuration

6.3 Simulation of the propagation of SPP waves through the ring-resonators

6.3.1 Source profile creation

The profile for the propagation of surface plasmon polariton (SPP) is created by having a Gaussian photon pulse incident on the metal-dielectric-metal interface on the input waveguide side. The normalized Ex, Ey and Hz fields for the generated SPP profile is shown in Fig. 6.8 and 6.9.

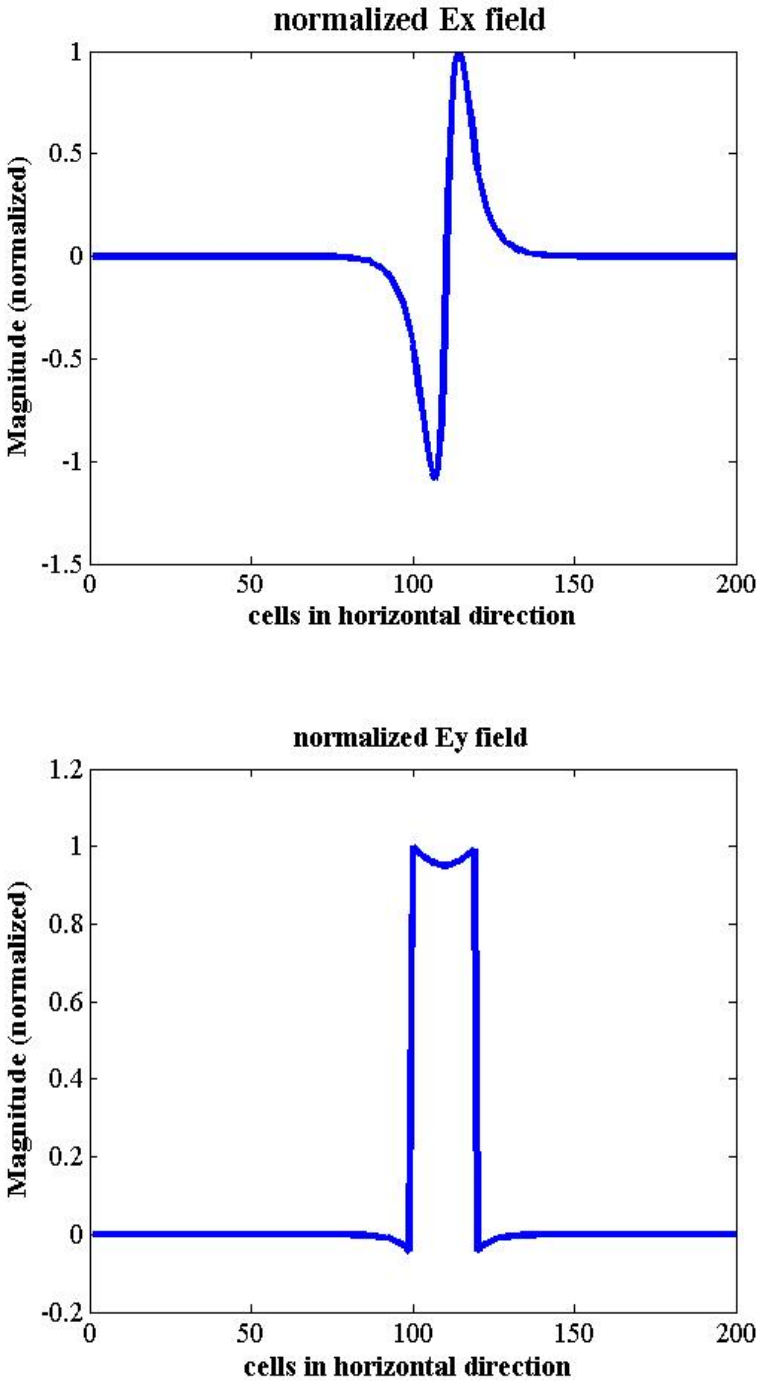

Fig 6.8: Ex and Ey profiles for the generated SPP wave

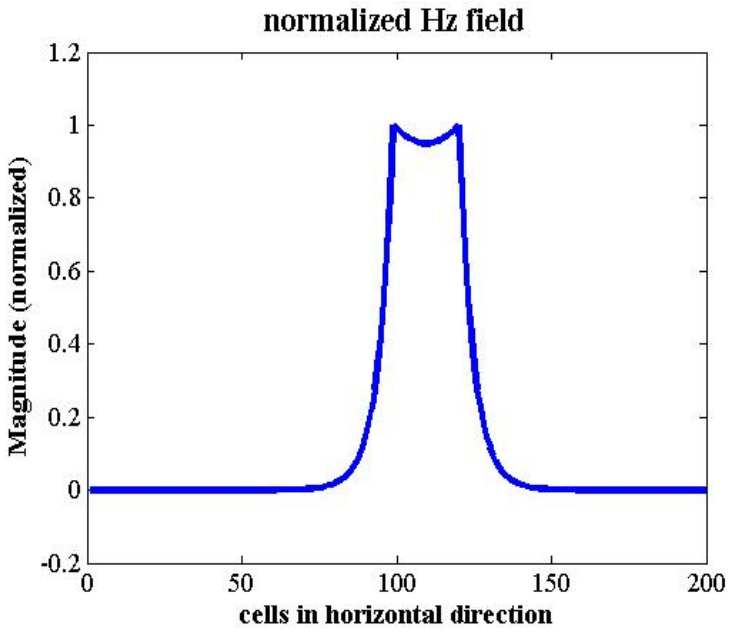

Fig 6.9: Hz profile for the generated SPP wave

The SPP wave profile obtained is incident at the input port of the first waveguide. Using the finite-difference-time-domain (FDTD) method and the material models obtained, the propagation of the SPP wave along the structures is simulated at different time intervals. To ensure complete convergence of the numerical analysis, very small grid sizes were chosen, with Δx=5nm and Δy=5nm. The simulation was carried out for 20000 time steps, to ensure the generated SPP wave reached a stable value. The time step is given by-

$$\Delta t = \frac{0.95}{c\sqrt{\frac{1}{\Delta x^2} + \frac{1}{\Delta y^2}}} \tag{5.11}$$

The plasmons propagate well without much loss along the dielectric waveguides composed of air, but the lossy silver medium causes the attenuation to the SPP waves as they propagate through it. The figures of the simulations for each of the add-drop ring resonator configurations are shown below. For each shape, the Hz field at resonant conditions, and the Hz field at non-resonant conditions is shown.

Circular ring

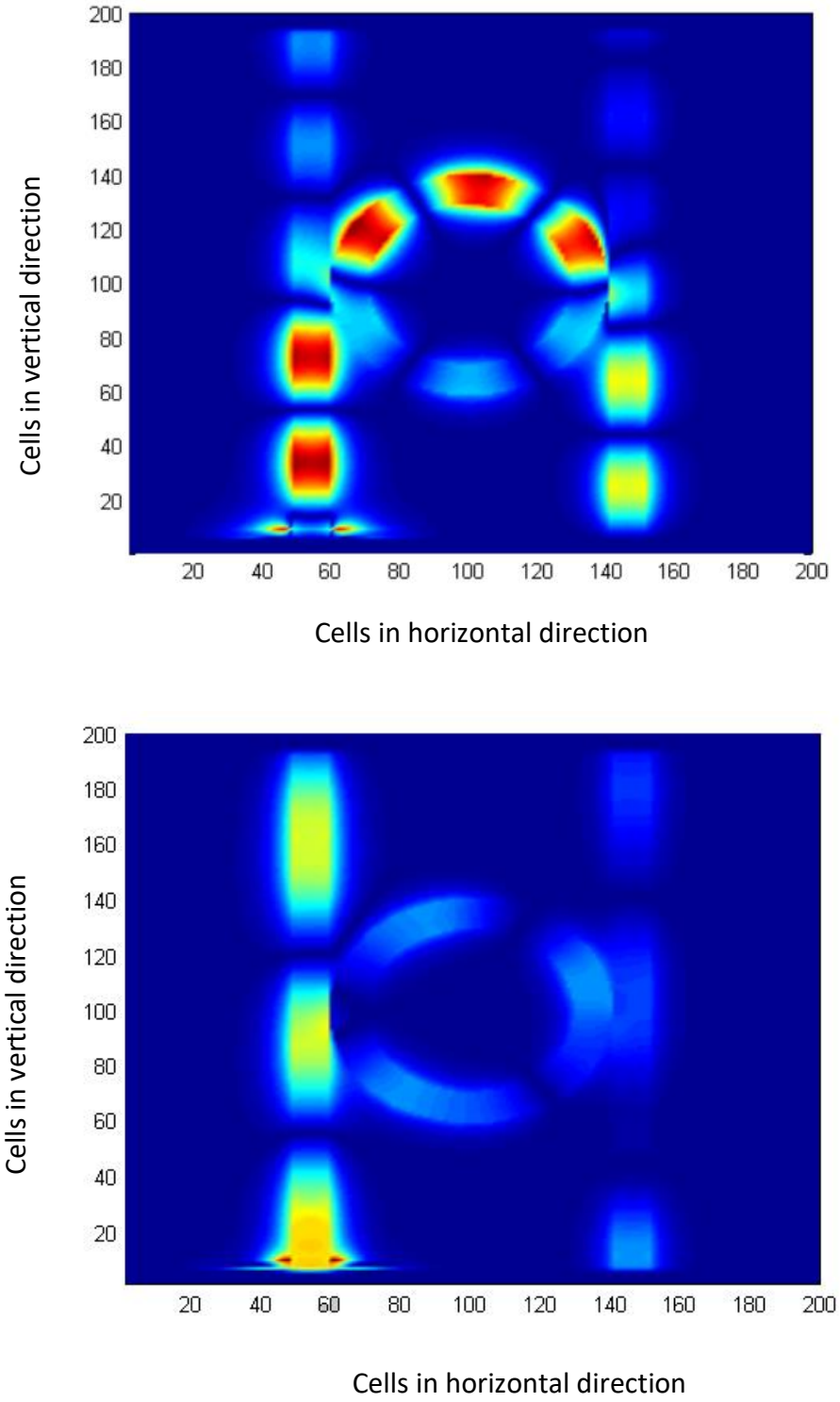

Fig 6.10: Hz field profiles for- a) Resonant condition, b) Non-resonant condition

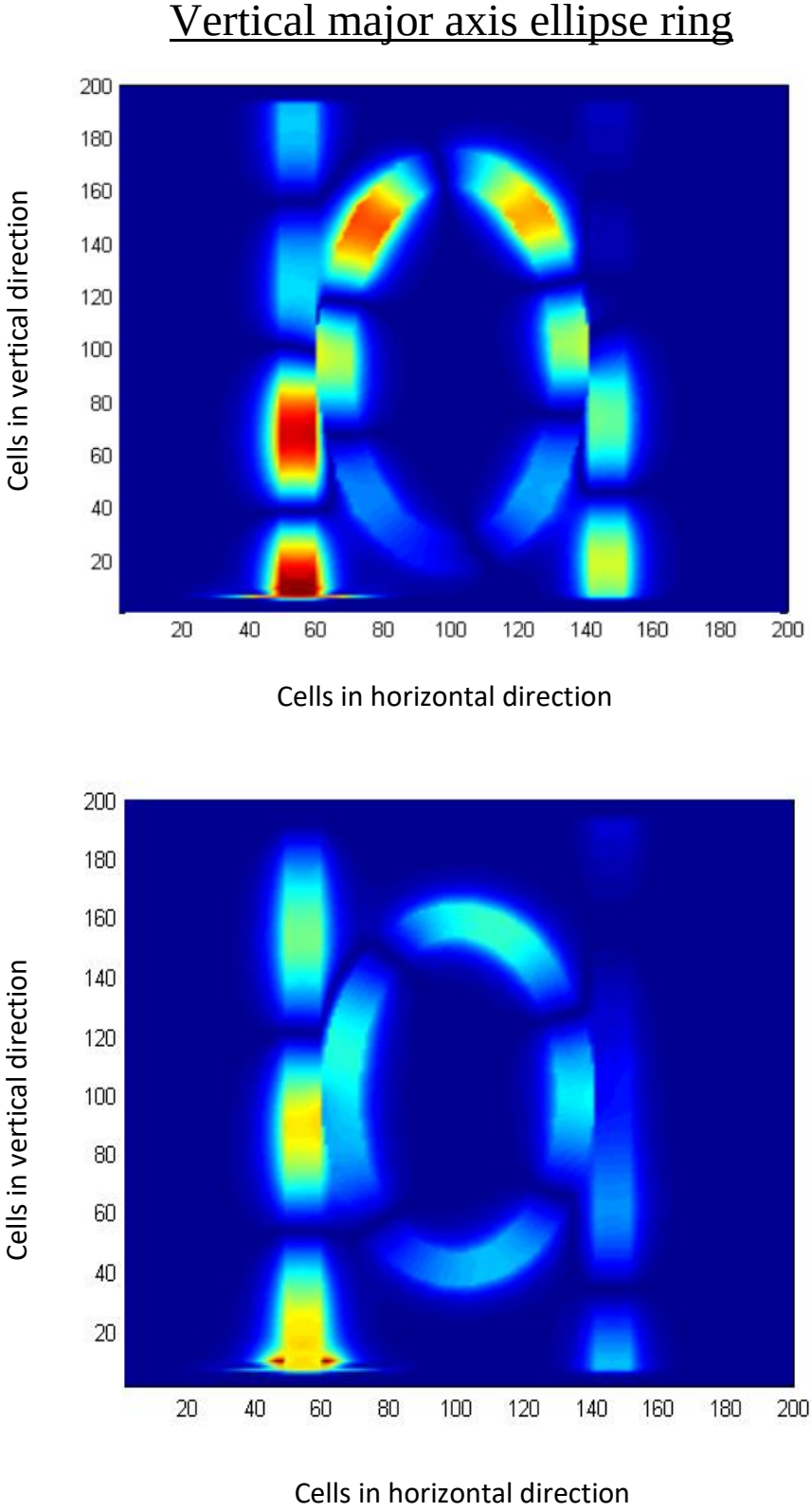

Fig 6.11: Hz field profiles for- a) Resonant condition, b) Non-resonant condition

Horizontal major axis ellipse ring

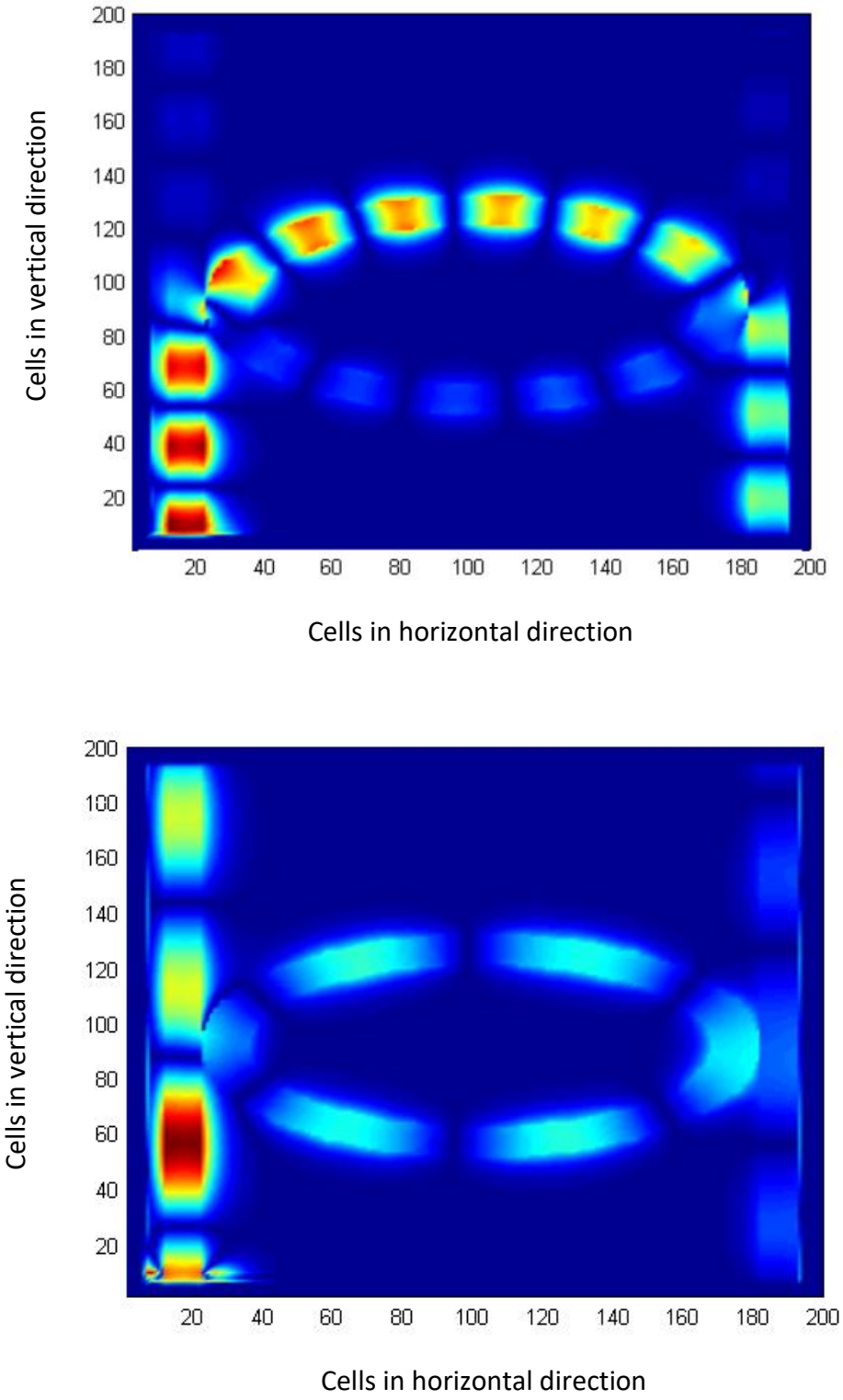

Fig 6.12: Hz field profiles for- a) Resonant condition, b) Non-resonant condition

Square ring

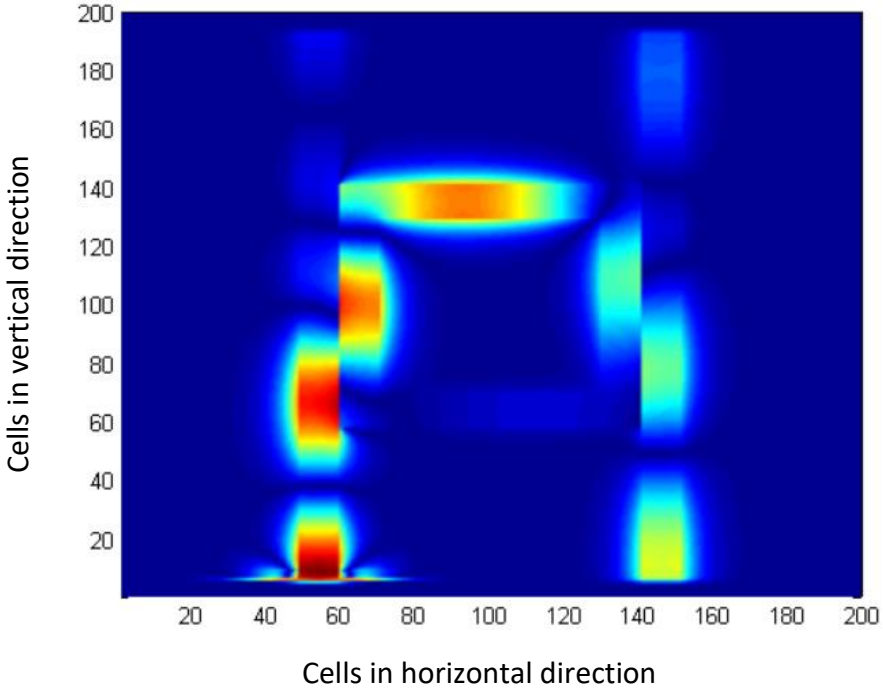

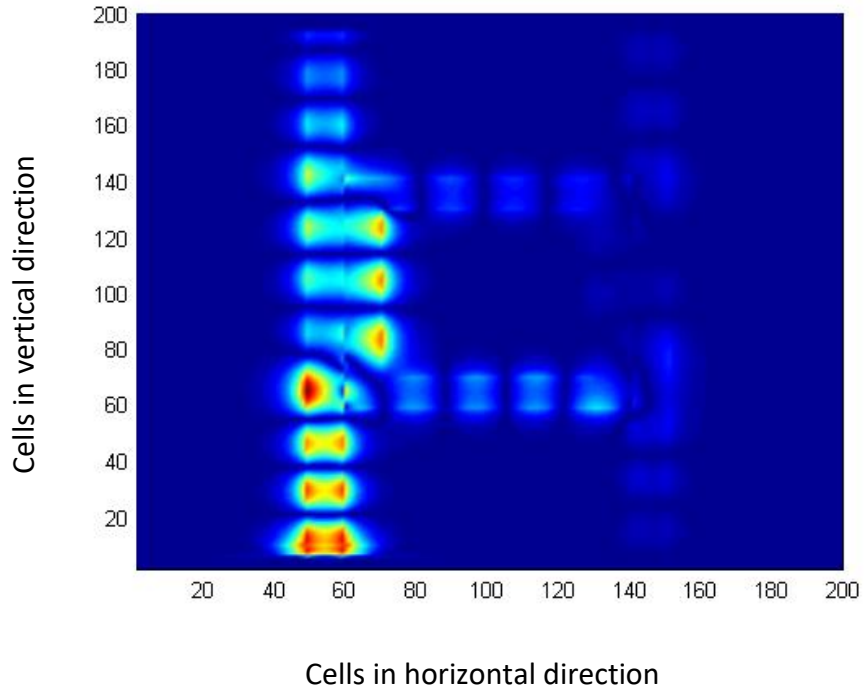

Fig 6.13: Hz field profiles for- a) Resonant condition, b) Non-resonant condition

Round-edge square ring

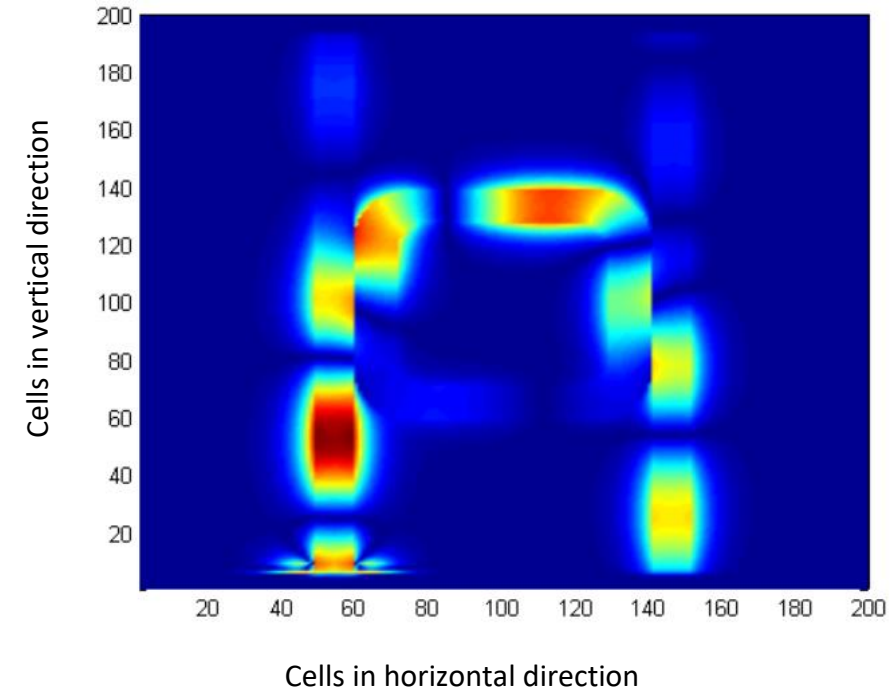

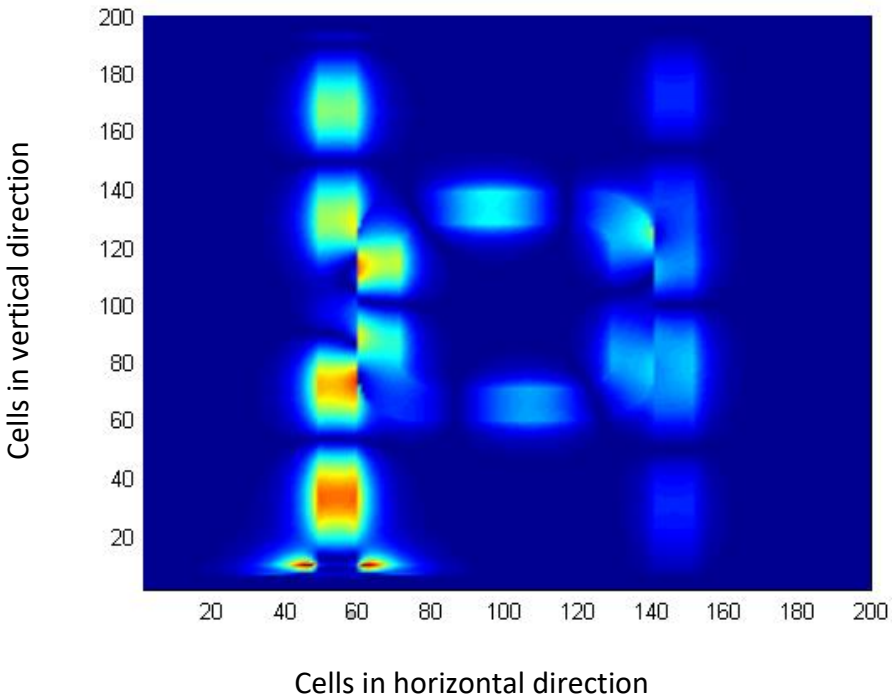

Fig 6.14: Hz field profiles for- a) Resonant condition, b) Non-resonant condition

Chapter 7

Results and their Analysis

7.1 Transmission characteristics

7.1.1 Overview

For an add-drop ring resonator, the transmission characteristics refer to the power at different ports of the resonator for different wavelengths of the input wave. At resonant conditions, maximum power is obtained at the drop port. Conversely, the power at the drop port is minimum under non-resonant conditions, since most of the power passes via the through port. The maximum power passing through the drop and through ports and the corresponding resonant frequencies gives a measure of the performance of a ring resonator and is referred to as the transmission characteristics of the device. We plotted the power at the drop and through ports vs wavelength to obtain the transmission characteristics of the different configurations.

7.1.2 Calculation of power at the ports

The power at the drop and through ports were calculated at different time steps. To calculate the power at different time steps, Poynting vector was used. Poynting vector is defined as the cross product of Electric and Magnetic field intensities at a certain instant or here, time step. Poynting vector formula is given by-

$$\vec{S} = \vec{E} \; X \; \vec{H} \qquad (5.12)$$

Where,

$\vec{S}$ = instantaneous power,

$\vec{E}$ = Electric field intensities

$\vec{H}$ = Magnetic field intensities

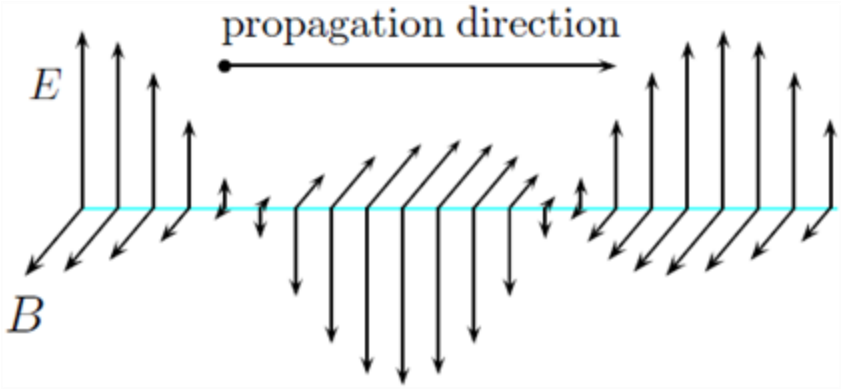

Fig 7.1: Direction of E and H fields for calculating instantaneous power.

The calculated power at the different ports were then divided by the input power at the input to obtain the transmission efficiency for each add-drop configuration.

7.2 Efficiency vs Wavelength curves for different ring shapes

7.2.1 Circular ring

The transmission efficiency at the drop and through ports was plotted vs wavelengths ranging from 700nm to 2500nm and is shown in Fig. 7.2.

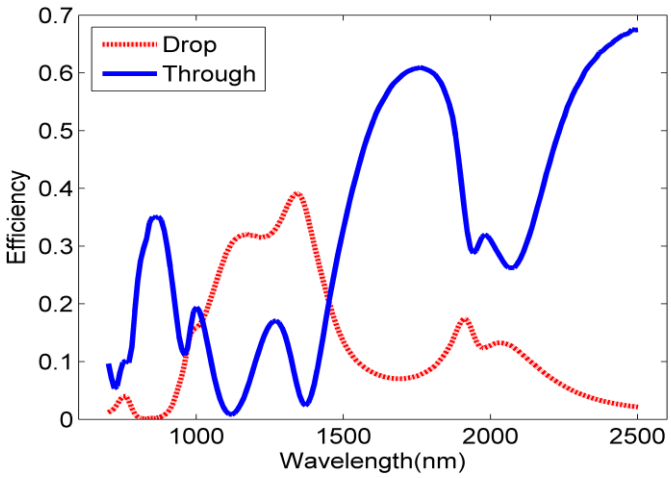

Fig 7.2: Efficiency vs Wavelength for circular ring

In the figure, the red curve represents the transmission characteristics of the drop port, and the blue curve represents that of the through port. It is seen that, generally, when the efficiency through the drop port is high for a particular wavelength, the corresponding efficiency at the through port is low. The maximum efficiency obtained at the drop port is 39% at a resonant wavelength of 1340nm. An additional resonant peak at a wavelength of 1900nm is also observed, with an efficiency of 17%.

7.2.2 Vertical major axis elliptical ring

The transmission characteristics are shown in fig 7.3.

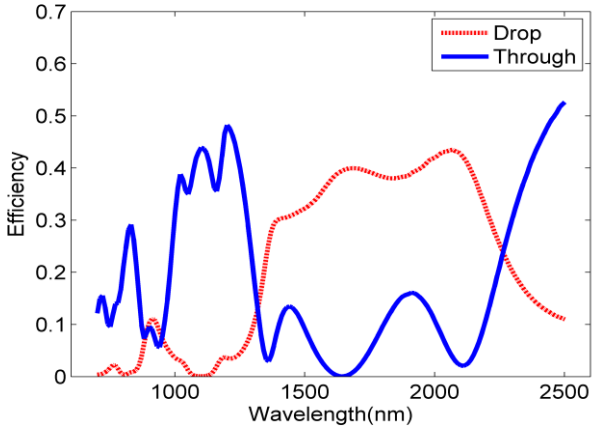

Fig 7.3: Efficiency vs wavelength for elliptical ring (vertical major axis)

For the elliptical ring, the maximum efficiency obtained is 44%, which is higher than the basic circular ring shape. The maximum efficiency occurs at a resonant wavelength of 2070nm. A close to ideal passband is observed between 1300nm and 2400nm, which means that this structure has potential use as a band-pass filter for this range of wavelengths.

7.2.3 Horizontal major axis elliptical ring

The transmission characteristics are shown in fig. 7.4.

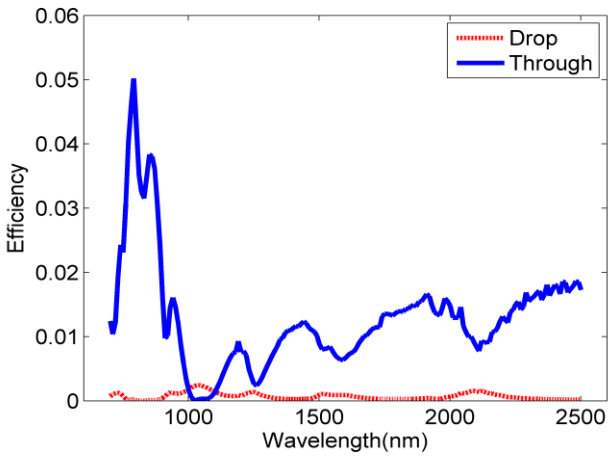

Fig 7.4: Efficiency vs wavelength for elliptical ring (horizontal major axis).

From the graph it is observed that for this range of wavelengths, most of the power passes via the through port. The maximum efficiency obtained is a negligible 0.24%.

7.2.4 Square ring

The transmission characteristics are shown in fig 7.5.

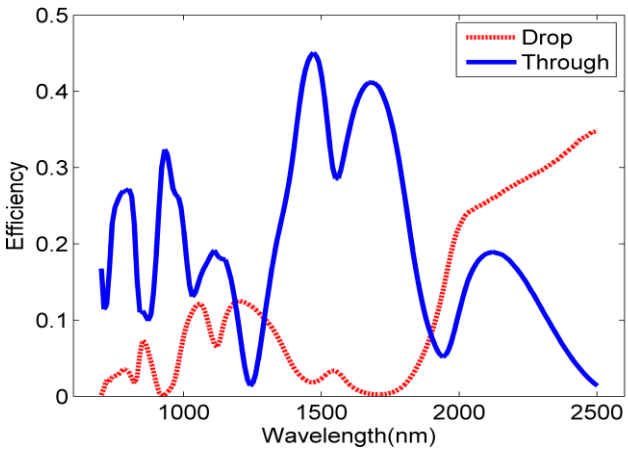

Fig 7.5: Efficiency vs Wavelength for square ring

The maximum efficiency obtained is 35% at a resonant wavelength of 2500nm. The part of the graph for the drop port between 1300nm and 1900nm represents something close to a stopband. This structure can be used as band-stop filter for this range of wavelengths, provided further modifications are made to enhance the stopband characteristics.

7.2.5 Round-edge square ring

The transmission characteristics are shown in fig 7.6.

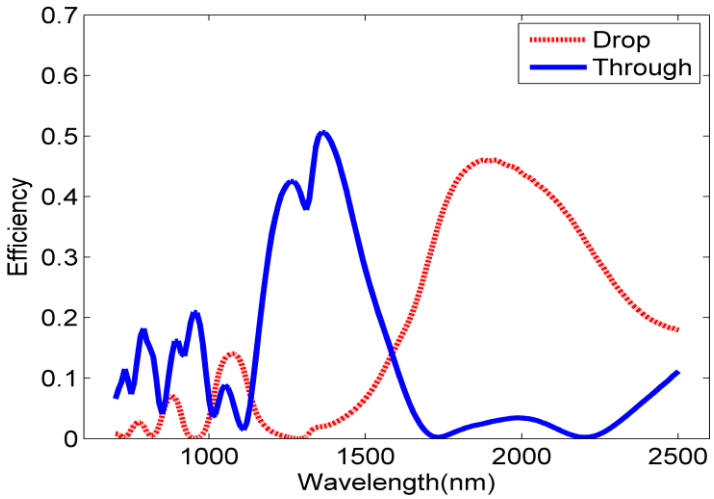

Fig 7.6: Efficiency vs Wavelength for round-edge square ring

The round-edge add-drop configuration shows the highest maximum efficiency at the drop port out of all the shapes, with an efficiency of 46% at a resonant wavelength of 1880nm. Two resonant peaks were also observed at wavelengths of 880nm and 1070nm, with efficiencies of 7% and 14% respectively.

7.2.6 Results

The transmission efficiency and the corresponding resonant wavelength for each of the shapes in summarized in Table 7.1.

Table 7.1: Maximum transmission efficiency of each ring resonator configuration and their corresponding resonant wavelengths.

Shape	Maximum transmission efficiency (%)	Resonant wavelength (nm)
Circular	39	1340
Ellipse (vertical major axis)	44	2070
Ellipse (horizontal major axis)	0.24	1040
Square	35	2490
Round-edge square	46	1880

7.3 Effect of coupling distance

7.3.1 Overview

The transmission characteristics were also observed by increasing the coupling distance between the input waveguide and the ring for each add-drop configuration. In the original simulations shown previously, the coupling distance, d, was kept at 5nm, as seen in fig. 6.3

to 6.7. Here, the coupling distance is increased to 20nm and its effect on the transmission efficiency is discussed.

7.3.2 Efficiency vs Wavelength curves

The graphs of efficiency vs wavelength for each geometric add-drop configuration is shown in fig 7.7(a) to fig 7.7(d). Simulations on the horizontal major axis ellipse configuration was not carried out since it already showed negligible drop port efficiency in the previous simulation.

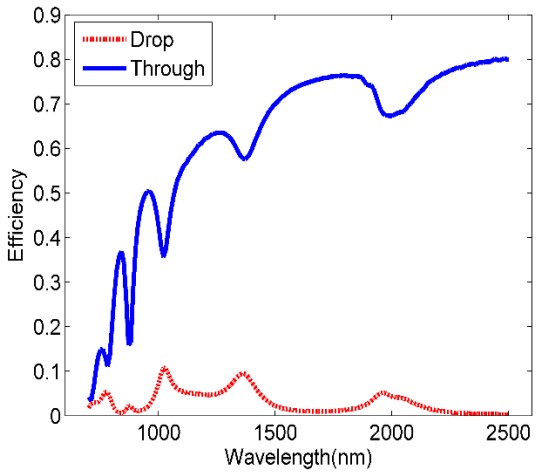

(a)

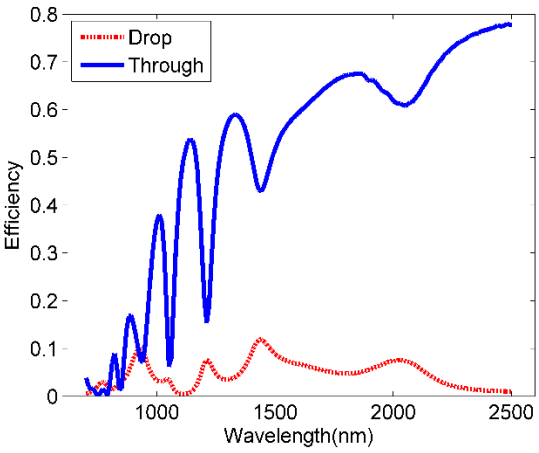

(b)

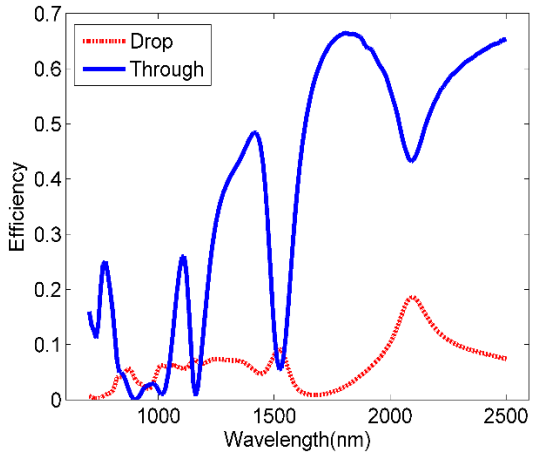

(c)

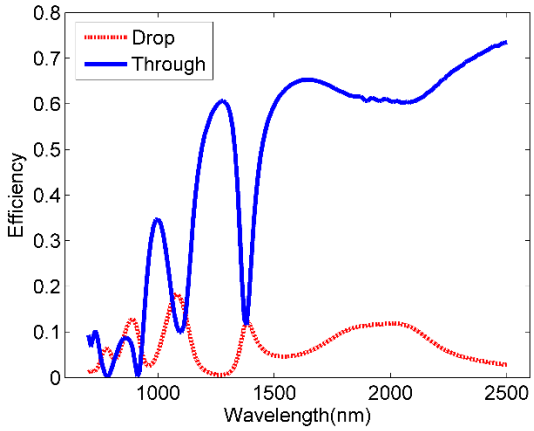

(d)

Fig 7.7(a)-7.7(d):- Transmission efficiency vs. Wavelength for, a) Circular, b) Ellipse (vertical major axis), c) Square, d) Round-edge square for a coupling distance of 20nm.

Here, it is observed that the maximum efficiency at the drop port decreases by more than double for each shape as a result of increasing the coupling distance from 5nm to 20nm. The normal square ring structure now has the highest maximum transmission efficiency of 18.6% at a resonant wavelength of 2090nm, while the circular ring resonator has the lowest with a maximum efficiency of 10.77% at a resonant wavelength of 1020nm.

The results are summarized in Table 7.2. It can be concluded that increasing the coupling distance significantly decreases the transmission efficiency at the drop port.

Table 7.2: Transmission efficiencies for increased coupling distance d=20nm

Shape	Maximum transmission efficiency (%)	Resonant wavelength (nm)
Circular	10.77	1020
Ellipse (vertical major axis)	12	1440
Square	18.6	2090
Round-edge square	18.31	1080

Chapter 8

Conclusion and future works

8.1 Conclusion

To summarize, we have proposed various geometric shapes for the ring in the add-drop ring resonator configuration in addition to the common circular ring and simulated and analyzed their transmission characteristics by using the propagation of SPP waves through an MDM waveguide interface. Our main aim was to determine which particular geometric structure for the ring has the optimum transmission efficiency and also the resonant wavelengths at which the transmission peaks occur. From our studies, we have found out that both the round-edge square (46%) and vertical major axis ellipse resonator (46%) structures show higher transmission efficiencies compared to the basic circular one (35%). We also investigated the change in the transmission characteristics by increasing the coupling distance between the input waveguide and the ring and observed that the transmission efficiency decreased significantly for each shape. From our studies, we can conclude that by utilizing the different transmission characteristics of different ring shapes, the design of filters, plasmonic diodes and various other plasmonic nanostructures can be optimized.

8.2 Future works

8.2.1 Optical NAND gate

The proposed structure of an optical NAND gate is shown in fig 8.1. The device has a typical Silicon on Insulator (SOI) structure with the waveguide and rings made out of silicon and placed on a silicon dioxide substrate. The device contains two main input ports, A and B, a control port C and an output port. The concept behind the design is that the input to the control port will always be HIGH and it will have twice the amplitude of the HIGH (1) input signal supplied to A and B and will be 180^0 out of phase with it. The frequency of the HIGH input signals used here will be the resonant frequency at which

each input signal resonates within their corresponding rings and will appear at their respective drop ports.

When both inputs A and B are zero, the control port is HIGH (1) and will result in a HIGH (1) output at the output port.

When either one of the inputs A and B is HIGH (1), it will superimpose with the control port input and will reduce the amplitude of C by half. A HIGH (1) output will still appear at output port equal to the value of the input signal at A or B.

When both A and B are on, they will superimpose with the control port input C and destructive interference will occur, resulting in a LOW (0) output at the output port.

So, the device performs similarly to a NAND gate combination who's expected results are summarized in table 3.

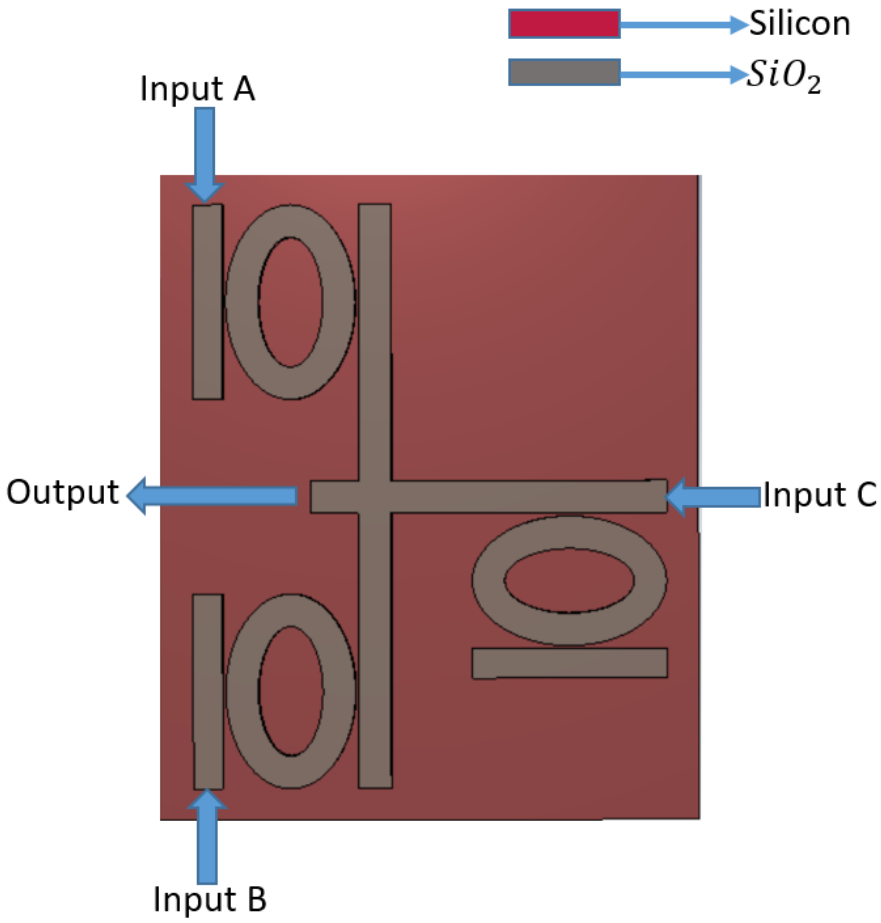

Fig 8.1 Proposed NAND gate structure

Table 3:- Expected truth table of proposed NAND gate

A	B	Control port	Output
0	0	1	1
0	1	1	1
1	0	1	1
1	1	1	0

8.2.2 Other works

We also have plans to work on other devices in the field of silicon photonics like the proposed NAND gate presented above and also improve and optimize the designed structures by further modifications and analysis. To give a more particular view of the planned future works, the following list is provided-

- To use the shapes with good transmission characteristics for designing devices suitable for various optical applications, like wavelength division multiplexing (WDM), coupled resonator optical waveguides (CROW) etc.
- To design other plasmonic devices like diodes, NOR, NOT logic gates etc.
- To use Computer Simulation Tool (CST) for improved and more efficient simulations of photonic structures.

References

[1] Alexandros Emboras, “Atomic scale plasmonic devices,” 18th international conference on Transparent Optical Networds, pp. 1-4, 2016.

[2] Tai Li, Lin Li, S, N, Zhu, “Steering surface plasmons on metal surface,” Conference on Lasers and Electro-Optics, pp. 1-2, 2012.

[3] Z. Ismail Khan, M. K. Mohd Salleh, Gaetan, Prigent, “Achievable bandwwidth of a quarter wavelength side-coupled ring resonator,” IEEE Symposium on Industrial Electronics & Applications, vol,1, pp. 358-361, 2009.

[4] H. A. Atwater, “The promise of Plasmonics,” Sci. Am., vol. 296, no.4, pp. 56-63, Apr. 2007.

[5] Stefan A. Maier, “Plasmonics: Metal nanostructures for subwavelength photonic devices,” IEEE Journal of Selected Topics in Quantum Electronics, vol. 12, issue. 6, pp. 1214-1220, 2006.

[6] Junchang Zhang, Liubiao Zhong, Jianmei Chen, Lin Jiang, “Plasmon-enhanced optoelectronic devices based on metal nanostructures,” Progress in Electromagnetic Research Symposium, pp.829-829, 2016.

[7] Chan Ho Kim, Kai Chang, Xiaoguang Liu, “Varactor tuned ring resonator filter with wide tunable bandwidth,” IEEE Radio & Wireless Symposium, pp. 141-143, 2015.

[8] Tsu-Wei Lin, Jen-Tsai Kuo, Shyh-Jong Kuang, “New miniaturized ring resonator bandpass filter with wide upper stopband,” IEEE MTT-S International Microwave Symposium Digest, pp. 1-4, 2013.

[9] M. A. M Muhammad, et al., “Multilayer structure of ring resonator filter for digital broadcasting,” International Conference on Computer Applications & Industrial Electronics, pp. 396-399, 2010.

[10] Hak-Sun Lee, Gun-Duk Kim, Sang-Shin Lee, “Temperature compensated refractometric biosensor exploiting ring resonators,” IEEE Photonics Technology Letters, vol. 21, pp. 1136-1136, 2009.

[11] Djafar. K. Mynbaev, Vitaly Sukharenko, “Plasmonics for optical communications: The use of graphene for optimizing coupling efficiency,” International Carribean Conference on Devices, Circuits & Systems, pp. 1-4, 2014.

[12] Linjie Zhou, et al., “Silicon active microring resonators for optical switching,” Progress in Electromagnetic Research Symposium, pp. 2621-2621, 2016.

[13] Xiao-yang Zhang, et al., “Tunable microring resonator based on dielectric-loaded surface plasmon polariton waveguides,” 3rd International Nanoelectronics Conference (INEC), p.1355-1356, 2010.

[14] Y. D. Zhang, H. Tian, X. N. Zhang, N. Wang, J. Zhang, H. Wu, and P. Yuan, “Experimental evidence of enhanced rotation sensing in a slowlight structure,” Opt. Lett. 35, 691-693, 2010.

[15] X. Q. Fan, “Silicon dual-ring modulator,” Opt. Express 17, 20783-20793, 2009.

[16] P. P. Absil, J. V. Hryniewicz, B. E. Little, R. A.Wilson, L. G. Joneckis, and P.-T. Ho, “Compact microring notch filters,” IEEE Phot. Technol. Lett. 12, 398-400, 2000.

[17] B. Liu, A. Shakouri, and J. E. Bowers, “Passive microring resonator coupled lasers,” Appl. Phys. Lett. 79, 3561–3563, 2001.

[18] L. Y. Mario and M. K. Chin, “Optical buffer with higher delaybandwidth product in a two-ring system,” Opt. Express 16, 1796-1807, 2008.

[19] Yundong Zhang, Kaiyang Wang, Xiaoqi Liu, Xuenan Zhang, “An add-drop ring resonator interferometer sensor with high sensitivity,” Seventh International Conference on Sensing Technology (ICST), pp.316-317, 2013.

[20] Arpita Sharma, Gloria Jospeh, “Add drop filter for CWDM systems using photonic crystal ring resonator,” International Conference on Advances in Engineering & Technology Research (ICAETR), pp. 1-3, 2014.

[21] Mirza Fuad Adnan and Hasibul Hasan, "Plasmonic resonances in hexagonal split-ring resonator," International Conference on Electrical, Computer and Communication Engineering (ECCE), 477-479, 2017.

[22] Yatinda Gaurav, Arvind Kumar Pandey, R. K. Chauhan, "Single notch band UWB BPF using square ring resonator," 3rd International Conference on Recent Advances in Information Technology (RAIT), 147-148, 2016.

[23] E. Verhagen, "Subwavelength light confinement with surface plasmon polaritons," 2009.

[24] H. Raether, Surface plasmons on smooth surfaces: Springer, 1988.

[25] A. Archambault, T. V. Teperik, F. Marquier, and J.-J. Greffet, "Surface plasmon Fourier optics," Physical Review B, vol. 79, p. 195414, 2009.

[26] E. Jin and X. Xu, "Plasmonic effects in near-field optical transmission enhancement through a single bowtie-shaped aperture," Applied Physics B, vol. 84, pp. 3-9, 2006.

[27] J. T. Krug II, E. J. Sánchez, and X. S. Xie, "Design of near-field optical probes with optimal field enhancement by finite difference time domain electromagnetic simulation," The Journal of chemical physics, vol. 116, pp. 10895-10901, 2002.

[28] W. H. Pernice, F. P. Payne, and D. F. Gallagher, "A general framework for the finite-difference time-domain simulation of real metals," Antennas and Propagation, IEEE Transactions on, vol. 55, pp. 916-923, 2007.

[29] A. D. Rakić, A. B. Djurišić, J. M. Elazar, and M. L. Majewski, "Optical properties of metallic films for vertical-cavity optoelectronic devices," Applied optics, vol. 37, pp. 5271-5283, 1998.

[30] M. A. Ordal, R. J. Bell, R. Alexander, L. Long, and M. Querry, "Optical properties of fourteen metals in the infrared and far infrared: Al, Co, Cu, Au, Fe, Pb, Mo, Ni, Pd, Pt, Ag, Ti, V, and W," Applied optics, vol. 24, pp. 4493-4499, 1985.

[31] G. Veronis and S. Fan, "Bends and splitters in metal-dielectric-metal subwavelength plasmonic waveguides," Applied Physics Letters, vol. 87, p. 131102, 2005.

[32] H. Gao, H. Shi, C. Wang, C. Du, X. Luo, Q. Deng, et al., "Surface plasmon polariton propagation and combination in Y-shaped metallic channels," Optics express, vol. 13, pp. 10795-10800, 2005.

[33] B. Wang and G. P. Wang, "Surface plasmon polariton propagation in nanoscale metal gap waveguides," Optics letters, vol. 29, pp. 1992-1994, 2004.

[34] G. Veronis and S. Fan, "Theoretical investigation of compact couplers between dielectric slab waveguides and two-dimensional metal-dielectric-metal plasmonic waveguides," Optics Express, vol. 15, pp. 1211-1221, 2007.

[35] P. Ginzburg and M. Orenstein, "Plasmonic transmission lines: from micro to nano scale with λ/4 impedance matching," Optics express, vol. 15, pp. 6762-6767, 2007.

[36] D. Pile and D. K. Gramotnev, "Adiabatic and nonadiabatic nanofocusing of plasmons by tapered gap plasmon waveguides," Applied Physics Letters, vol. 89, p. 041111, 2006.

[37] R. Wahsheh, Z. Lu, and M. Abushagur, "Nanoplasmonic air-slot coupler: design and fabrication," in Frontiers in optics, 2012.

[38] R. Luebbers, F. P. Hunsberger, K. S. Kunz, R. B. Standler, and M. Schneider, "A frequency dependent finite-difference time-domain formulation for dispersive materials," Electromagnetic Compatibility, IEEE Transactions on, vol. 32, no. 3, pp. 222–227, 1990.

[39] D. F. Kelley and R. J. Luebbers, "Piecewise linear recursive convolution for dispersive media using FDTD," Antennas and Propagation, IEEE Transactions, vol. 44, no. 6, pp. 792–797, 1996.

[40] R. J. Luebbers, F. Hunsberger, and K. S. Kunz, "A frequency-dependent finite-difference time-domain formulation for transient propagation in plasma," Antennas and Propagation, IEEE Transactions on, vol. 39, no. 1, pp. 29–34, 1991.

[41] A. Akyurtlu and D. H. Werner, "Bi-FDTD: A novel finite-difference time-domain formulation for modeling wave propagation in bi-isotropic media," Antennas and Propagation, IEEE Transactions on, vol. 52, no. 2, pp. 416–425, 2004.

[42] A. Grande, I. Barba, A. C. Cabeceira, J. Represa, P. P. So, and W. J. Hoefer, "FDTD modeling of transient microwave signals in dispersive and lossy bi-

isotropic media," Microwave Theory and Techniques, IEEE Transactions on, vol. 52, no. 3, pp. 773-784, 2004.

[43] A. Akyurtlu and D. H. Werner, "A novel dispersive FDTD formulation for modeling propagation in chiral metamaterials," Antennas and Propagation, IEEE Transactions, vol. 52, no. 9, pp. 2267–2276, 2004